

# Paleoceanography and Paleoclimatology

## RESEARCH ARTICLE

10.1029/2019PA003809

### Key Points:

- Sediment provenance is used as indicator of palaeoceanographic changes in northeast Baffin Bay
- Detrital proxies reveal a stronger influence of the West Greenland Current after ~7.7 cal ka BP
- Variations in sediment provenance on the northwestern margin are interconnected to regional ice streams activity

### Supporting Information:

- Supporting Information S1

### Correspondence to:

M. Caron,  
myriam.caron03@uqar.ca;  
caron.myriam11@gmail.com

### Citation:

Caron, M., Montero-Serrano, J.-C., St-Onge, G., & Rochon, A. (2020). Quantifying provenance and transport pathways of Holocene sediments from the northwestern Greenland margin. *Paleoceanography and Paleoclimatology*, 34. <https://doi.org/10.1029/2019PA003809>

Received 5 NOV 2019

Accepted 1 MAR 2020

Accepted article online 4 MAR 2020

## Quantifying Provenance and Transport Pathways of Holocene Sediments From the Northwestern Greenland Margin

Myriam Caron<sup>1</sup> , Jean-Carlos Montero-Serrano<sup>1</sup> , Guillaume St-Onge<sup>1</sup> , and André Rochon<sup>1</sup>

<sup>1</sup>Institut des sciences de la mer de Rimouski, GEOTOP, Université du Québec à Rimouski, Rimouski, Québec, Canada

**Abstract** The mineralogical and geochemical compositions of three sediment cores from the northwestern Greenland continental margin (AMD14-204 and AMD14-210) and Kane Basin (AMD14-Kane2B) were investigated using quantitative X-ray diffraction and energy-dispersive X-ray fluorescence in order to document the impact of ice-ocean interactions on the sediment provenance and transport pathways during the Holocene. Unmixing of the sediment composition and ratios such as quartz/clays and K/Fe indicate that detrital sediments in cores from the northwest Greenland margin are derived mainly from Prøven granite and reworked Archean gneiss, whereas sediments from Kane Basin are derived mainly from detrital carbonate (Ellesmere Island) and Proterozoic gneiss (Humboldt Glacier). Mineralogical and geochemical signatures also reveal that changes in detrital sediment provenance and transport in the region are strongly interconnected to regional ice stream dynamics, especially during the early Holocene with strong meltwater discharge from the Greenland Ice Sheet associated with the end of deglaciation. With the establishment of milder conditions during the mid-Holocene and reduced glacial activity once ice sheets retreated inland, sediment inputs via ocean currents became more effective. Thus, detrital proxies in core AMD14-204, located in the Upernavik cross-shelf trough, support the hypothesis of an intensification of the West Greenland Current influence after 7.7 cal ka BP, which eventually affected the regional sediment dynamic by a greater contribution from basalt to the sediment supply. Finally, our results suggest that the interactions between climate, glacial dynamics, and surface ocean circulation controlled the paleoenvironmental changes observed in the three cores.

## 1. Introduction

During the last few decades, the Arctic has strongly responded to modern climate warming with the rapid rate of retreat and thinning of the Greenland Ice Sheet (GIS; e.g., Howat et al., 2008; Joughin et al., 2008, 2016; Rignot et al., 2010, 2016; Straneo & Heimbach, 2013; Winsor et al., 2015), as well as a strong intensification of ice mass loss for the Canadian Arctic Archipelago (CAA) ice sheets (Miller et al., 2005; Noël et al., 2018; Pendleton et al., 2019) and sea ice (Serreze & Stroeve, 2015). A better understanding of the interactions between sea ice, ice caps, and climate throughout the geological past can be valuable to place these modern changes into perspective and to understand their natural variability (Jakobsson et al., 2010; Müller & Stein, 2014).

Baffin Bay is an excellent location to study climate-ocean-ice dynamics mostly for its proximity to the GIS and CAA ice caps (Figure 1). During the Last Glacial Maximum (LGM), the GIS was ~65% more enlarged than present (Funder et al., 2011) and extended to the continental shelf edge (e.g., Ó Cofaigh, Dowdeswell, et al., 2013). Consequently, the expansive West Greenland shelf (WGS) is marked by large troughs extending seaward up to the continental slope, and trough-mouth fans are observed along the shelf break (e.g., Aksu & Piper, 1987; Batchelor & Dowdeswell, 2014; Ó Cofaigh, Dowdeswell, et al., 2013, 2018; Jakobsson et al., 2012). Because of their potential for rapid sediment accumulation, these cross-shelf troughs are excellent locations to study paleoenvironmental changes at a high temporal resolution (multicentury), as they can record past glacial (and deglacial) conditions (e.g., Dowdeswell et al., 2014; Jennings et al., 2014). Thus, they can help to better document and reconstruct the ice margin dynamics and their links with the major oceanographic and climatic changes that occurred since the last deglaciation.

In addition, the study of late Quaternary sediments from the Baffin Bay have provided important information to distinguish (i) variations in the provenance of detrital particles (Andrews et al., 2014, 2018; Sheldon

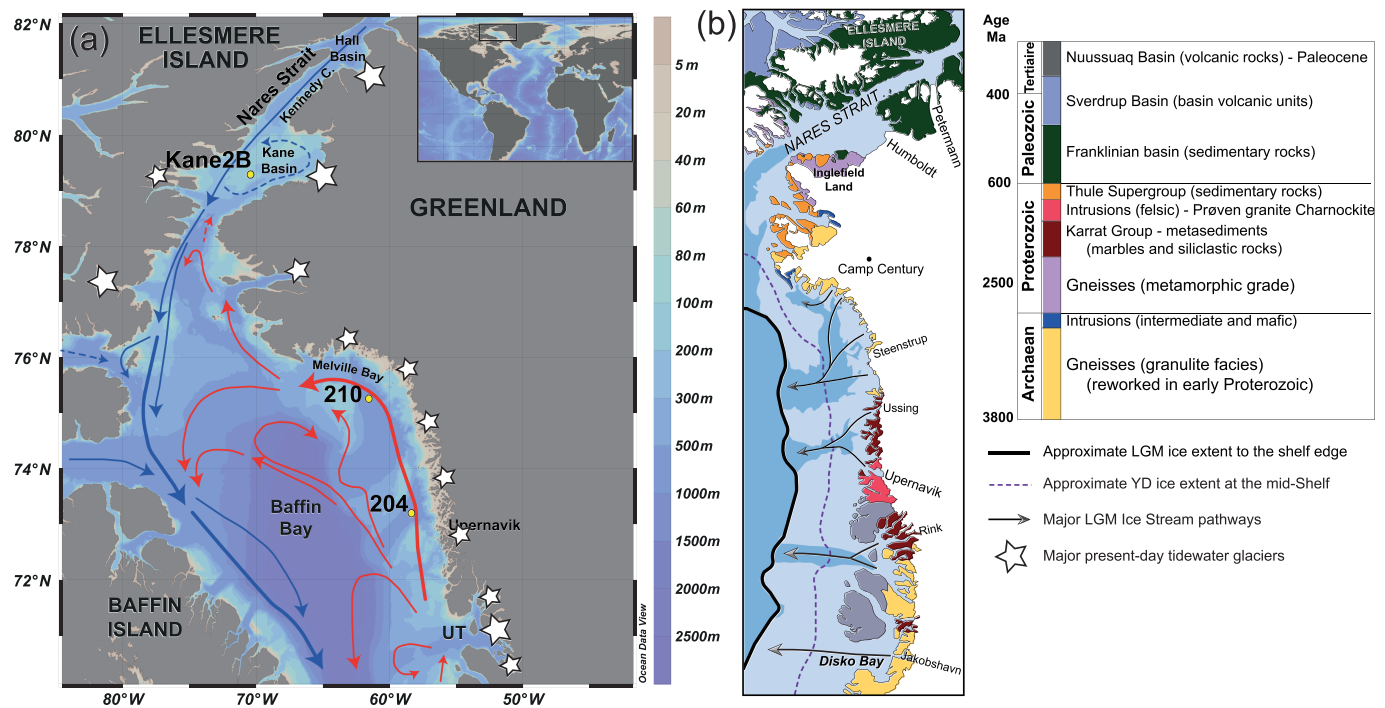


**Figure 1.** (a) Map of Baffin Bay with general surface circulation (West Greenland Current or WGC in red and Baffin Island Current or BIC in blue) and locations of the three sediment cores studied herein. UT: Ummannaq trough. (b) Simplified geological map of the Baffin Bay surroundings inspired from geus.dk interactive geological map (Escher & Pulvertaft, 1995) and limits of the Greenland Ice Sheet (GIS), Last Glacial Maximum (LGM), and Younger Dryas (YD) ice extent based on Slabon et al. (2016) and Batchelor et al. (2018).

et al., 2016; Simon, 2013; Simon et al., 2014, 2016), (ii) climate and atmospheric changes in source regions and surrounding land masses (e.g., Andrews & Jennings, 2014; Thomas et al., 2016), and (iii) variations in sediment propagation and ocean current trajectories (e.g., Georgiadis et al., 2018; Jennings et al., 2017; Simon, 2013). In this regard, the present study proposes new mineralogical and geochemical data from three marine sediment cores recovered from the Upernavik cross-shelf trough (AMD14-204), Melville Bay cross-shelf trough (AMD14-210), and Kane Basin (AMD14-Kane2B). These results are used here to assess the contributions from specific sediment sources, evaluate the transport processes of detrital sediment, and provide new insights on potential relations between Holocene climatic variability, oceanic circulation variations, and sediment dynamics along the northwestern Greenland margin. A comparison with previously published sedimentological and palynological data from the same cores (Caron, St-Onge, et al., 2019; Caron, Rochon, et al., 2019; Georgiadis et al., 2018) permitted to acquire a large overview of the paleoenvironmental changes occurring in these regions during the Holocene. Thus, our study differs from earlier publications with this multiproxy approach, which provides an opportunity to improve the regional knowledge of the environmental changes of the northwestern Greenland margin and Nares Strait during the Holocene. Moreover, it helps improve the discrimination of regional sediment sources (Baffin Bay and Nares Strait) in order to better reconstruct sediment dynamics evolution during the Late Quaternary (Andrews, 2019).

## 2. Geological and Environmental Setting

Baffin Bay is an oceanic basin 1,300 km long and 4,50 km wide located between Greenland, Baffin Island, and the CAA with a maximum depth of up to 2,300 m (Aksu & Piper, 1987). The shallow Kane Basin (water depth up to 250 m) is part of NE-SW orientated Nares strait that connects the Arctic Ocean and Baffin Bay (Figure 1a). The bedrock geology of western Greenland is generally characterized by the presence of the Precambrian Shield, which is composed of metamorphic and igneous rocks dated from Archaean and Proterozoic (Figure 1b). Rocks outcropping in NW Greenland, along the shores of the Melville Bay, are largely dominated by reworked Archean orthogneiss (granulite facies metamorphic grade) and are part of the

Rinkian mobile belt (Oakey & Chalmers, 2012; Pedersen & Pulvertaft, 1992). An early Proterozoic sedimentary formation (metasediments) called the Karrat Group (Henderson & Pulvertaft, 1967; Kalsbeek et al., 1998) is overlaying these reworked Archaean gneisses (Figure 1b). Moreover, around the fjord of Upernavik (Figure 1), Precambrian Charnockites (orthopyroxene-bearing granites; Escher & Pulvertaft, 1995) outcrop and are part of the Prøven Igneous Complex (Thrane et al., 2005). These Charnockites intruded in the center of the Rinkian mobile belt (reworked Archaean gneisses) and in the middle of the Karrat Group (Henderson & Pulvertaft, 1967; Kalsbeek et al., 1998; Figure 1b). In northern Greenland, early Proterozoic gneisses outcrop at the southern border of Humboldt Glacier (Inglefield mobile belt). North of Humboldt Glacier and on Ellesmere Island, a Paleozoic sedimentary carbonate-bearing rock formation (the Franklinian Basin) is overlaying the Precambrian Shield (Figure 1b; Hiscott et al., 1989; MacLean et al., 1990). Other Proterozoic sedimentary rocks are also outcropping in the northwestern part of Greenland and southern part of Ellesmere Island (surrounding Smith Sound) and form the Thule Supergroup (e.g., Dawes, 1997). At the end of the Cretaceous and early Tertiary, Greenland and North America were separated by the formation of rifts, which disconnected the Precambrian cratons (e.g., Dawes, 2009; Dawes et al., 2000; MacLean et al., 1990). The development of large grabens and basaltic lava flows (Palaeogene) along the Canadian and Greenlandic margins (basaltic and picritic eruptions into a low-lying coastal environment), in the region of Disko and Ummannaq Bays, was associated to this rifting (Figure 1b; Escher & Pulvertaft, 1995; Larsen & Pedersen, 2009).

The bathymetry of Baffin Bay is asymmetrical, with a central abyssal plain surrounded by the large Greenland continental shelf (250 km) to the east, and a much narrower Baffin Island continental shelf (25–50 km) to the west (Andrews et al., 2014; Tang et al., 2004). These continental shelves were geologically shaped by the large GIS, Laurentian (LIS), and Inuitian (IIS) Ice Sheets during the most recent and previous glaciations, as demonstrated by the presence of cross-shelf trough systems that extend from the coast and out to the continental slope (e.g., Aksu & Piper, 1987; Ó Cofaigh, Dowdeswell, et al., 2013; Slabon et al., 2016). Indeed, the alternation of glacial and interglacial periods through time has strongly affected Baffin Bay and the Arctic Ocean more largely (e.g., Hiscott et al., 1989; Simon, 2013). During the LGM, the junction of the three large ice sheets, LIS, IIS, and GIS, blocked the straits of the CAA, preventing the flow of polar water to the Baffin Bay (Dyke, 2004; Dyke et al., 2002; England et al., 2006). The opening of Nares Strait (~9.0–8.3 cal ka BP; Georgiadis et al., 2018; Jennings et al., 2019) permitted the connection between the Arctic and North Atlantic Oceans through Baffin Bay, allowing the development of the modern oceanic circulation in Baffin Bay and in Labrador Sea (e.g., Georgiadis et al., 2018; Jennings et al., 2011, 2019). On the WGS, marine geophysical and geological data provided evidence that extended GIS reached the shelf edge during the LGM (e.g., Ó Cofaigh, Andrews, et al., 2013; Jennings et al., 2017, 2018; Slabon et al., 2016). Initial grounding line retreat from the shelf edge likely occurred between 13.8 and 15 cal ka BP along central WGS (Ó Cofaigh, Andrews, et al., 2013; Jennings et al., 2017; Sheldon et al., 2016), and there is evidence of a still stand during the Younger Dryas (YD, 12.9–11.7 cal ka BP), then followed by a rapid final retreat (e.g., Batchelor et al., 2018; Briner et al., 2013; Funder et al., 2011; Slabon et al., 2016).

Baffin Bay is a pathway for freshwater and sea-ice transport between the Arctic and North Atlantic oceans. The oceanic circulation in Baffin Bay is counter-clockwise, fed by relatively warm and salty water flowing north through Davis Strait, forming the West Greenland Current (WGC), and by a strong surface current of polar water (cold and fresh) flowing through CAA straits (Barrow and Nares Straits), forming the Baffin Island Current (BIC; Figure 1a; Tang et al., 2004). The WGC is flowing at intermediate depth and is a mixture of the East Greenland Current (cold and fresh water originating from the Arctic through Fram Strait) and the Irminger Current (warm and salty water originating from the Atlantic Ocean) that join south of Greenland. Most of the WGC flowing northward turns west in the Melville Bay region to join the BIC, flowing southward along Baffin Island toward the Labrador Sea (Tang et al., 2004). Sedimentation in Baffin Bay is affected by the presence of numerous icebergs and meltwater inputs originating from the GIS, especially through major glaciers such as Jakobshavn Isbrae, Rink, Steenstrup, and Humboldt Glaciers (Figure 1b; e.g., Rignot et al., 2010). Most of the icebergs present in Baffin Bay are produced by the West Greenlandic ice streams and especially in the two most productive regions: Disko and Ummannaq Bays (Tang et al., 2004). Icebergs produced in the Disko Bay area will leave Baffin Bay through Davis Strait, while most of the icebergs produced north of Disko Bay can drift with the WGC up to the north of Baffin Bay then bifurcate toward the south along the Canadian coast (Tang et al., 2004). Thus, present-day

sediments found in Baffin Bay seafloor are mainly derived from glacial erosion of the surrounding Greenland and CAA land masses through various sedimentary processes (such as ice rafting debris or IRD, glaciogenic debris flows, meltwater plumes, and turbidity currents) that are dominant in these glaciated environments (e.g., Andrews et al., 1998, 2014, 2018; Hiscott et al., 1989; Marlowe, 1966; Ó Cofaigh et al., 2003; Simon et al., 2014).

### 3. Materials and Methods

#### 3.1. Core Setting, Chronology and Lithological Description

Three Calypso Square cores were collected on board the Canadian Coast Guard Ship icebreaker Amundsen along the northwest Greenland margin during the ArcticNet (Leg 1b) expedition in July 2014. Cores AMD14-204 and AMD14-210 (hereinafter referred to as 204 and 210) are located on the northwest Greenland margin, in the cross-shelf troughs west of Upernavik Isstrøm, and in Melville Bay, respectively, whereas core AMD14-Kane2B (hereinafter referred to as Kane2B) is located in the Kane Basin (Figure 1 and Table 1). Core Kane2B age model was calibrated using a regional reservoir correction of  $\Delta R = 240 \pm 51$  (Georgiadis et al., 2018, 2020), while age models for cores 204 and 210 were calibrated using a regional age reservoir correction of  $\Delta R = 140 \pm 30$  (Caron, St-Onge, et al., 2019). These  $\Delta R$  values were selected based on previous regional studies (Jackson et al., 2017; Jennings et al., 2014; Lloyd et al., 2011; Moros et al., 2016), and age models were validated with palaeomagnetic data (Caron, St-Onge, et al., 2019). An improved version of core 204 age model was established with the addition of organic matter dating (J. Giraudeau, personal communication, December 2019). The chronostratigraphic framework, sedimentation rates, CT scan images, and sedimentary units of the three cores are presented in Figure S1 in the supporting information (Caron, St-Onge, et al., 2019; Georgiadis et al., 2018, 2020).

Four main lithofacies were identified and described in the three cores (Caron, St-Onge, et al., 2019) and represent distinctive sediment delivery processes and probable provenance changes during the Holocene (e.g., Jenner et al., 2018). These facies are (1) glaciomarine, ice-proximal conditions, resulting in moderate to high concentrations of IRD; (2) glaciomarine conditions in which deposition of suspended sediments from turbid meltwater plumes is a dominant process; (3) progressive establishment of ice distal conditions reflected by alternation of different sedimentation processes (stratification); and (4) bioturbated hemipelagic sedimentation with little to no ice-rafting activity (see Caron, St-Onge, et al., 2019, for additional information on the lithofacies and their environmental interpretations). The terrigenous fraction of these late Quaternary sediments is originating from the weathering of different bedrock sources, which can be identified by comparing their mineralogical and geochemical signatures (e.g., Andrews et al., 2018; Andrews & Eberl, 2011).

#### 3.2. Mineralogical and Geochemical Analyses

The three cores were sampled every 8 cm ( $n = 92$  for core 204,  $n = 72$  for core 210, and  $n = 53$  for core Kane2B; mean resolution of 100–200 years). Prior to mineralogical and geochemical analyses, the sediment samples (<2-mm fraction) were rinsed 5 times with distilled water after the removal of the organic matter fraction with 10 ml of hydrogen peroxide (30%  $H_2O_2$ ) and biogenic carbonates with 10 ml of hydrochloric acid (HCl; 0.5 M). Note that detrital carbonates (notably, dolomite) are not removed following this attack, as suggested by its detection in the bulk sediment XRD diffractograms (Figure S2). Next, sediment samples were oven-dried overnight at approximately 60 °C and then slightly homogenized with an agate mortar. Aliquots of these homogenized samples were used for geochemical and bulk mineralogical analyses.

##### 3.2.1. Quantitative Bulk Mineralogy

Bulk mineral associations were studied by quantitative X-ray diffraction (qXRD) following the method developed by Eberl (2003), which was successfully used in other Quaternary glacial marine studies for

**Table 1**  
*Location of the Sampling Sites, Water Depth, and Length of the Cores Used in This Study*

Station	Latitude (°N)	Longitude (°W)	Region	Water depth (m)	Core length (cm)
AMD14-204	73°15.663'N	57°53.987'W	Upernavik	987	734
AMD14-210	75°24.317'N	61°39.357'W	Melville Bay	1,155	596
AMD14-Kane 2B	79°30.908'N	70°49.742'W	Kane Basin	220	425

descriptions of sediment mineralogy in the Baffin Bay (e.g., Andrews, 2019; Andrews et al., 2015, 2018; Jennings et al., 2019; Ó Cofaigh, Andrews, et al., 2013; Sheldon et al., 2016). For this, ~1 g of each sample (<2 mm) was spiked with 0.25 g of corundum and then ground in a McCrone micronizing mill using 5 ml of ethanol to obtain a homogenous powder. Next, 0.5 ml of vertrel was added to the mixture to prevent the possible agglomeration of finer particles. The powder sample is then sieved (<300  $\mu\text{m}$ ), back loaded into the holders, and analyzed on a PANalytical X'Pert powder diffractometer. The diffractometer scanned the samples from 5 to 65° two-theta in steps of 0.02° two-theta, with a counting time of 4 s per step. For the quantification of the major mineralogical components, sediment XRD scans obtained were converted into mineral weight percent (wt.%) using the Excel macro program ROCKJOCK v11 (Eberl, 2003). This program uses a full-pattern fitting method that permits the quantification of whole-sediment mineralogy with a precision of  $\pm 3$  wt.% (Eberl, 2003). The calculated total mineral wt.% was normalized to a sum of 100%. Selected minerals in ROCKJOCK are minerals expected to be found in the sediments, but some of these minerals were grouped, such as the various feldspars (e.g., Andrews & Vogt, 2014). We focused on 13 key minerals—quartz (Qz), K-feldspar (Kfs), plagioclase (Pl), calcite (Cal), dolomite (Dol), pyroxene (Px), amphibole (Am), Fe-bearing, amorphous silica (A. Silica), kaolinite (Kln), smectite (Sme), illite (Ill), chlorite (Chl), and biotite (Bt)—that represented more than 95% of the overall mineral concentration in the bulk sediment samples (data available online, Caron, Montero-Serrano, et al., 2019).

### 3.2.2. Bulk Elemental Concentration

Elemental compositions of sediments were analyzed by energy-dispersive X-ray fluorescence (ED-XRF) spectrometry, using a PANalytical Epsilon 3-XL. We considered a total of 14 elements (Al, Si, K, Mg, Ca, Ti, Mn, Fe, P, Sr, V, Cr, Zn, and Zr) with analytical procedures similar to Gamboa et al. (2017) and Deschamps et al. (2018). Prior to ED-XRF analysis, loss on ignition was determined gravimetrically by heating the dried samples up to 950 °C for 3 hr. Then, ~0.6 g of samples was treated by borate fusion in an automated fusion furnace (CLAISSE® M4 Fluxer) to form glass disks, prior to being analyzed with the spectrometer. Following the analysis, acquired ED-XRF spectra were processed with the standardless Omnia software package (PANalytical) (data available online, Caron, Montero-Serrano, et al., 2019). Procedural blanks always accounted for less than 1% of the lowest concentration measured in the sediment samples. Analytical accuracy and precision were found to be better than 1–5% for major elements and 5–10% for the other elements, as checked against an international standard (USGS SDC-1) and analysis of replicate samples.

### 3.2.3. Statistical Approach

Principal component analysis (PCA) was performed on the mineralogical and elemental geochemical datasets with the goal of finding associations with similar relative variation patterns that may be interpreted from a paleoenvironmental standpoint (e.g., Gamboa et al., 2017; Montero-Serrano et al., 2010; von Eynatten et al., 2003, 2016). A linear discriminant analysis (LDA) was also performed with the potential sediment sources in order to demonstrate the different mineralogical composition of these sources (Figure 2). Prior to all multivariate analyses, a log-centered (clr) transform was applied to the data (Aitchison, 1990). This operation removes statistical constraints on compositional variables, such as the constant-unit sum, and allows the valid application of classical (Euclidean) statistical methods to compositional data (e.g., Aitchison, 1990; Montero-Serrano et al., 2010). PCA and ternary plots were conducted using the “CoDaPack” software (Comas & Thió-Henestrosa, 2011), which automatically applies a log-centered (clr) transformation to the data, whereas the LDA was performed using the PAST software (Hammer et al., 2001).

### 3.2.4. Sediment Sources and Unmixing Model

In order to gain a quantitative understanding of the downcore changes in bulk sediment provenance, we used the nonlinear unmixing Excel macro program SedUnMixMC (Andrews et al., 2015; Andrews & Eberl, 2012). The program uses a Monte Carlo approach to randomly sample ( $n = 100$ ) the available source samples, defines a degree of fit between the observed and calculated mineral (raw data), and calculates a standard deviation on the estimates for each sample and each source. We ran SedUnMixMC on the normalized (100%) data for the 12 key minerals (Table 2) that represented more than 99% of the overall mineral concentration in the sediment samples. As summarized in Andrews et al. (2014, 2018), modern sediment inputs in the northwestern Greenland margin are mainly derived from West Greenland (including potential source areas: Disko Bay, Upernavik, Melville Bay) and the CAA (notably, Ellesmere Island). Moreover, Andrews et al. (2018) determined four groups of modern surface sediment samples associated to different sources areas from the West Greenland margin, called “West Greenland Mineral Cluster” (WGMC), which we

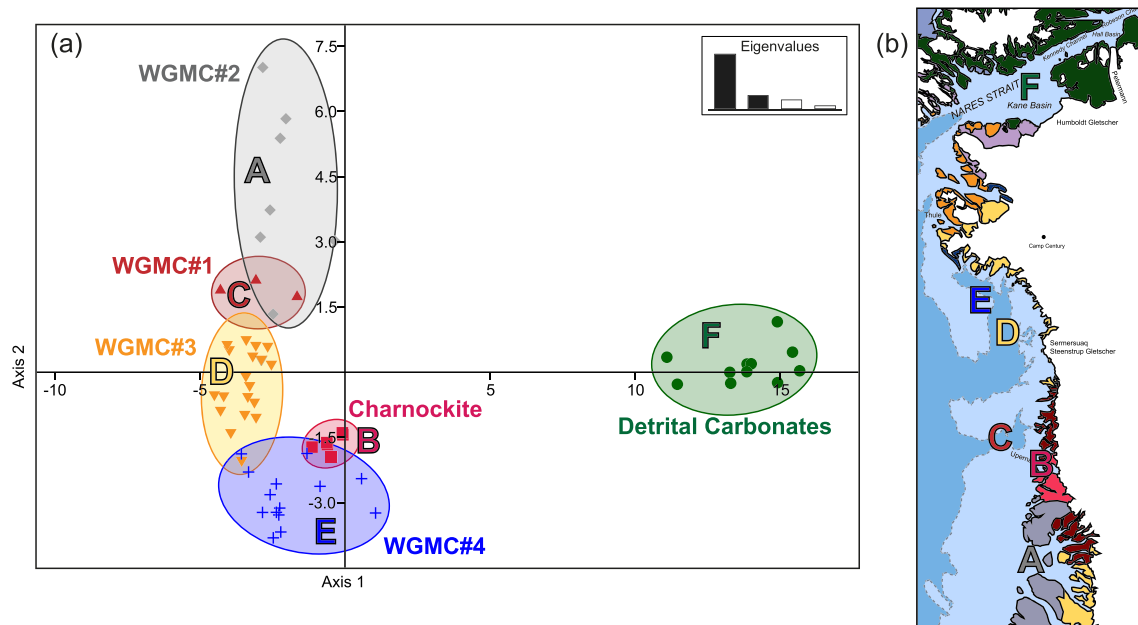


**Figure 2.** (a) Linear discriminant analysis of the main sediment sources used for this study. West Greenland Mineral Cluster (WGMC) and Upernavik (Charnockite) data are from Andrews et al. (2018) and Cordua (2016), respectively. These sediment sources were then used in the SedUnMixMC modeling. (b) Map of the approximative provenance areas for the sediment sources discussed in this study: basalts (A, WGMC#2), Upernavik charnockite (B), Karrat Group (C, WGMC#1), Precambrian Shield (D and E, WGMC#3 and #4), and detrital carbonates (F). Note that 93.2% of the cluster memberships are correctly classified (Table S1).

used here as potential sediment sources for the studied core locations during the Holocene. Four glaciomarine sediment samples from the Upernavik fjord (Cordua, 2016) were processed here for qXRD and also used as additional potential sources (Figure 2). Note that qXRD data from WGMC were obtained using zincite as a calibration spike (Andrews et al., 2018). However, comparison between the previous method using zincite (Rockjock v6) and the new method using corundum (Rockjock v11; as used in this study) has been previously discussed (e.g., Andrews et al., 2013; Andrews & Vogt, 2014) with no significant differences observed.

Based on these, we ran the SedUnMixMC using the following potential sediment sources: (A) basalts (Nuussaaq Basin, rich in pyroxene, plagioclase feldspars, and iron-bearing minerals, WGMC#2; Andrews

**Table 2**  
Average Mineralogical Composition for the Main Sources Used in the SedUnMix Modeling and Discussed in This Study

	Detrital (n = 11)	carbonates	Upernavik (n = 4)	charnockite	WGMC#1 (n = 3)	WGMC#2 (n = 7)	WGMC#3 (n = 11)	WGMC#4 (n = 7)				
Minerals present	Average	SD	Average	SD	Average	SD	Average	SD	Average	SD		
Quartz	14.56	6.01	21.83	1.90	5.67	0.81	12.33	5.88	11.11	4.01	27.81	5.08
K-Feldspar	6.64	3.82	21.59	1.28	10.43	0.12	8.64	2.30	14.16	1.44	15.43	2.33
Plagioclase	6.53	2.25	26.20	0.89	24.93	0.90	31.30	4.40	28.63	2.71	33.39	2.86
Carbonates	39.25	10.47	0.18	0.13	0.57	0.15	1.01	0.51	0.49	0.25	1.03	0.78
Amphibole	0.88	0.44	0.18	0.20	1.97	0.06	1.97	0.33	2.90	0.64	3.44	0.46
Pyroxene	0.49	0.40	1.35	1.06	2.67	0.45	9.51	5.12	1.10	0.76	0.56	0.28
Fe-bearing	0.46	0.59	0.72	0.37	2.20	0.26	4.47	1.31	1.05	0.55	0.66	0.56
A. Silica	5.99	2.30	1.09	0.92	12.60	0.82	9.31	1.80	12.15	2.03	10.21	1.66
Kaolinite	1.22	2.47	0.01	0.00	1.20	0.26	0.59	0.52	0.95	0.59	0.21	0.20
Smectite	3.09	2.90	1.68	1.18	14.83	1.96	7.97	5.05	9.27	3.67	0.13	0.05
Illites	13.14	7.74	9.84	1.47	8.30	1.14	4.59	1.63	6.15	1.12	2.51	1.20
Biotite and chlorite	8.84	1.96	15.08	2.23	11.50	0.66	6.97	1.71	10.54	2.43	4.24	1.37

Note. WGMC (West Greenland Mineral Cluster) and detrital carbonate data are from Andrews et al. (2018), while Upernavik data are from this study and Cordua (2016). A. Silica: amorphous silica.

et al., 2018); (B) Proven granite/charnockite from Upernavik (high content of quartz, feldspars plagioclase, and pyroxene; Cordua, 2016); (C) metasediments (Karrat Group, rich in plagioclase, smectite, and biotite and chlorite; WGMC#1; Andrews et al., 2018); (D and E) NW Greenland sources (Precambrian Shield): (D) mineral cluster #3 (WGMC#3) dominated by feldspars and clays minerals, notably smectite, illites, and biotite and chlorite; (E) mineral cluster #4 (WGMC#4) dominated by quartz and feldspars (Andrews et al., 2018); and (F) detrital carbonates (Franklinian Basin, dominated by detrital calcite and dolomite; Andrews et al., 2018). The main sources of carbonate-rich sediments are located in NW Greenland and the CAA (e.g., Parnell et al., 2007) and more specifically from north-east Ellesmere Island and northernmost Greenland (surrounding Nares Strait; Figure 1b). In agreement with Andrews et al. (2018) and Andrews (2019), the LDA (Figure 2) indicates that the six potential sources used in this study have minerals that allow a reasonable degree of sediment discrimination (average mineral composition shown in Table 2). In this context, we chose to run SedUnMixMC using samples from the following sources: (A), (B), and (C) for core 204; (B), (D), and (E) for core 210; and (D), (E), and (F) for core Kane2B (Figure 2 and Table 2). Andrews et al. (2018) and Andrews (2019) have previously suggested that the most useful minerals in discriminating sources in the Baffin Bay regions were plagioclase, dolomite, pyroxene, amphibole, smectite, and illites. As examples, dolomite can be used to track sediments originating from Ellesmere Island and North Greenland (“Detrital carbonates”), while pyroxene can be used to track sediments originating from the Disko/Uummannaq Bay area (“Basalts”). Likewise, gneiss from Inglefield Land is mainly of the Granulite metamorphic facies (dominated by feldspars, quartz, and orthopyroxene), while gneiss from Melville Bay is mainly of the amphibolite metamorphic facies (dominated by amphibole and plagioclase).

## 4. Results

### 4.1. Mineralogical and Geochemical Associations

Boxplot of the relative abundance of the main mineral used in this study for the three sediment cores (Figure 3a) illustrates the relatively similar composition of cores 204 and 210 compared to core Kane2B. Indeed, cores 204 and 210 have similar weight (wt.%) mineral distributions, dominated by quartz (~8–14%), K-feldspar (~8–13%), and plagioclase (~25–32%), whereas core Kane2B is distinguished by higher values of quartz (~23–26%), calcite and dolomite (~17–22%). This is coherent, given the location of core Kane2B in a small basin, close to the Paleozoic carbonate-rich sediments from Ellesmere Island and Northern Greenland (Parnell et al., 2007). Likewise, the ternary plot of the three most abundant minerals (quartz, plagioclase, and K-feldspar) shown in Figure 3c also reveals the mineralogical correspondence of core 204 with core 210, both largely dominated by a West Greenland mineralogical source, while core Kane2B mostly corresponds to a source rich in detrital carbonates. Furthermore, the ternary plot of detrital carbonates (calcite and dolomite), amphibole, and pyroxene (Figure 3d) reveals a mineral composition more abundant in pyroxene in core 204, whereas core 210 is rich in amphibole. The grain size distribution for the three cores reflects a composition generally dominated by silts and clays (Figure 3b). Overall, those plots illustrate different sediment sources for the three cores, as well as some apparent changes of provenance throughout the cores.

The geochemical composition (ED-XRF) for the three cores (Figure 4a) confirms the relatively similar composition of cores 204 and 210 compared to core Kane2B (especially with Mg, Al, and Ca). In addition, because aluminosilicates and clay minerals are largely associated with Al, quartz with Si and carbonates are associated with Ca, the ternary plot Al-Si-Ca (expressed as oxides; Figure 4b) was used to obtain a general geochemical classification of the sediments (e.g., Deschamps et al., 2018; Gamboa et al., 2017). This complementary diagram shows that the elemental sediment composition also reflects the major distinction between sedimentary sources for core Kane2B (rich in detrital carbonates) and for cores 204 and 210 (similar to average shale; Pourmand et al., 2012). Moreover, the elongated disposition of samples in core Kane2B reveals the strong variability, likely reflecting a carbonate dilution by a variable contribution in aluminosilicates and quartz-rich sediments during deposition. In addition, Fe-K-Ca ternary plot (Figure 4c) indicates dissimilarities between cores 204 (dominated by Fe) and 210 (dominated by K), while core Kane2B is dominated by Ca. These geochemical differences may be related to different sediment sources, such as K-rich gneisses, Fe-rich charnockite/basalts, and Ca-rich detrital carbonates (Figure 4c).

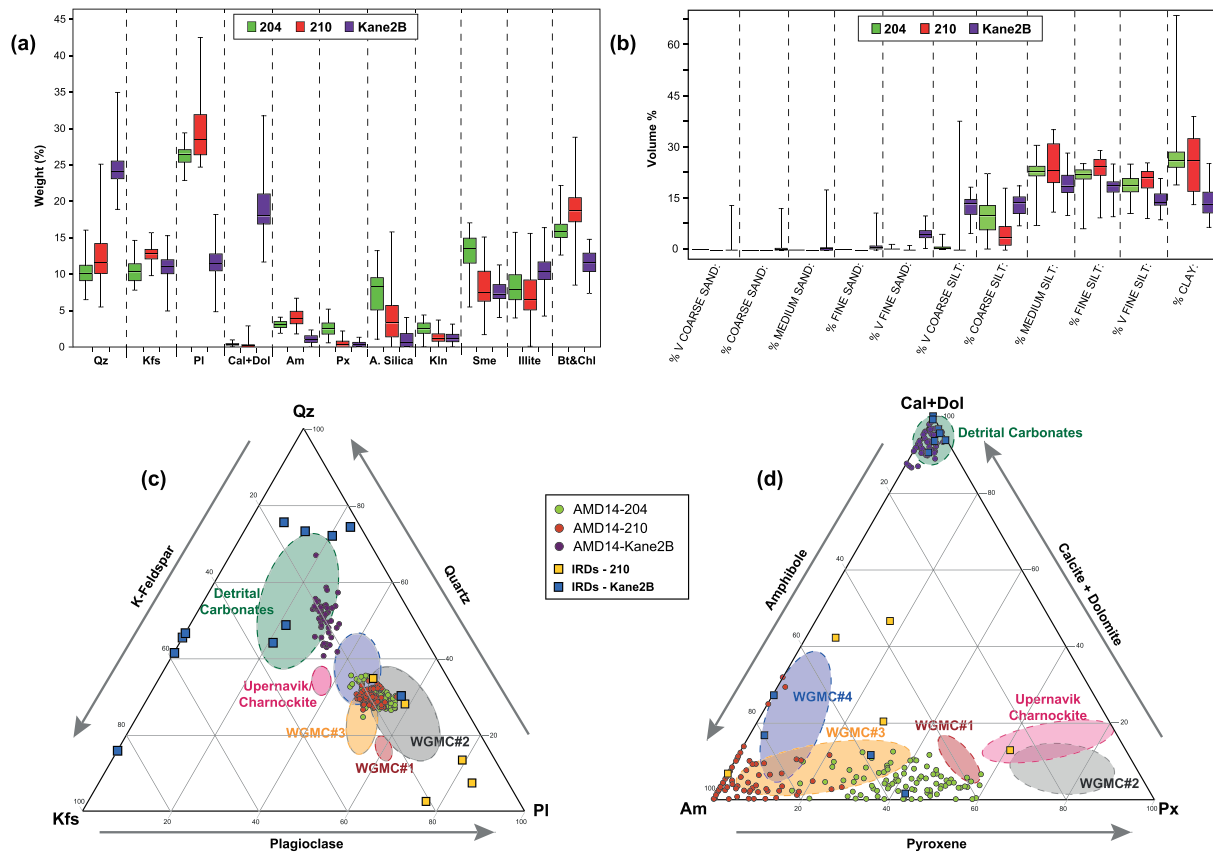


**Figure 3.** Results of mineralogical composition (quantitative X-ray diffraction) for the three cores 204, 210, and Kane2B with: (a) boxplot of the distribution of the main minerals (wt.%) within the cores, (b) boxplot of the grain size distribution (%) for the three cores, (c) quartz-K-feldspar-plagioclase, and (d) carbonate-amphibole-pyroxene ternary plots. The colored ellipses represent mineralogical signatures from the main sources discussed in this study (Andrews et al., 2018; this study).

In order to have a better understanding of the different mineral and geochemical associations and to choose how to associate them with the different sediment sources, PCA were conducted on all sediment cores (Figures S3). For the three cores, the first two principal components for both qXRD and ED-XRF accounted for about 90–95% of the total variance and results were distinguished based on the sedimentary units determined by Caron, St-Onge, et al. (2019). Mineralogical and geochemical associations were established for the three cores based on these results. In core 204, Unit 1 was associated with quartz, K-feldspar, biotite and chlorite, and Al-K-Zn-Sr, while Unit 2 was associated with pyroxene, smectite, amphibole, and Ca-Mg-Ti-Fe (Figure S3). Thus, we selected the quartz/smectite, K-feldspar/pyroxene, Ca/Al, K/Fe, and Al/Ti ratios to reconstruct downcore changes in sediment provenance and transport during the Holocene. These ratios provide straightforward proxies to discriminate the sediments from the Upernavik/Charnockite (rich in quartz and feldspars), basalts (rich in pyroxene and plagioclase), or WGMC#1 (rich in feldspars and smectite) in core 204. In core 210, Unit 1 was associated with quartz, plagioclase, amphibole, and Si-Fe-Ca; Unit 2a was associated with amphibole, biotite and chlorite, and Mg-Fe; and Units 2b and 3 were associated with smectite and Ti-Mg-Al (Figure S3). Therefore, we selected the quartz/clays, smectite/plagioclase, K/Fe, Fe/Al, and Ti/Al ratios to discriminate sediments from the Melville Bay sources (mostly orthogneiss and ultramafic rocks: WGMC#3, rich in plagioclase and clay minerals, and WGMC#4, rich in quartz and feldspars). Finally, in core Kane2B, Unit 1 is associated with calcite, feldspars, and Ti-Ca-Mg, Unit 2 is associated with feldspars, amphibole, smectite, and K-Al-Ca, while Unit 3 is associated with quartz, detrital carbonates, biotite and chlorite, illite, and Ca-Mg-Ti (Figure S3). Hence, we selected the quartz/plagioclase, calcite/feldspars, Mg/Al, Ca/Al,

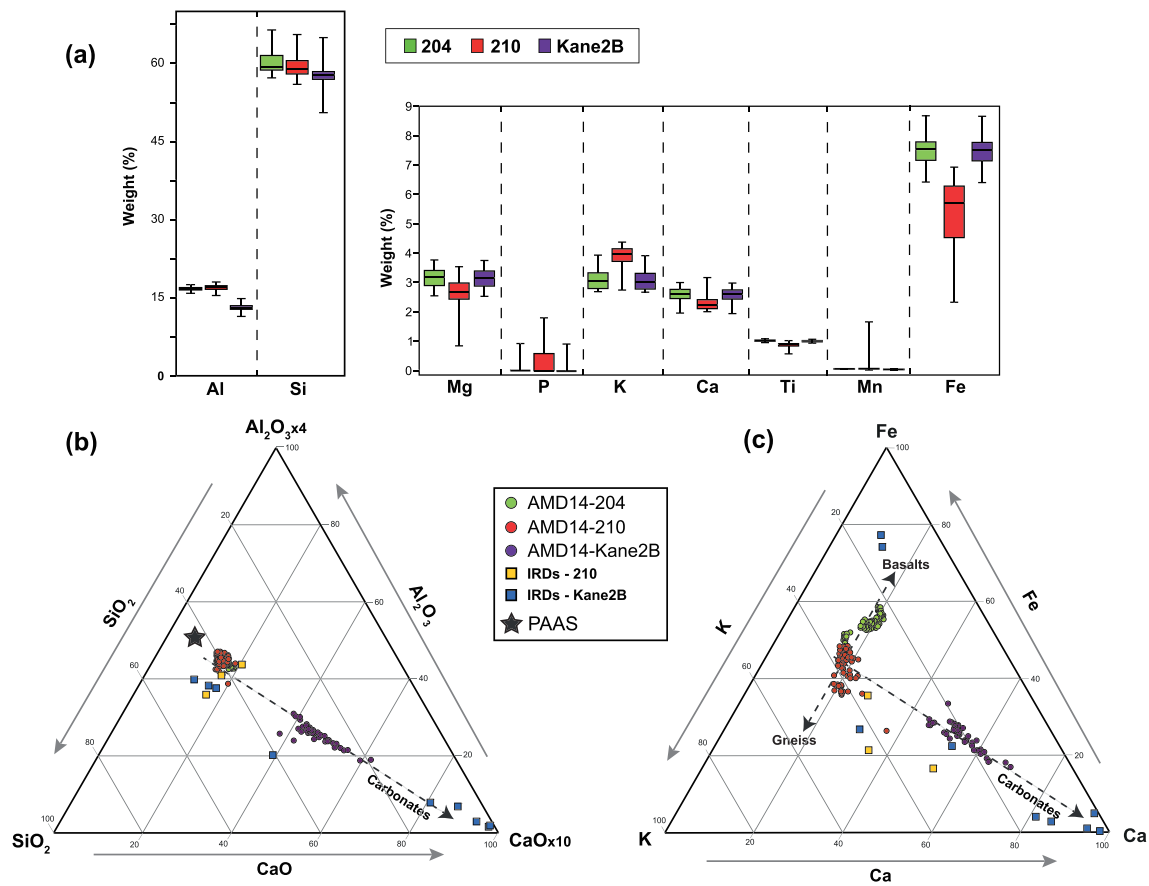


**Figure 4.** Results of the geochemical composition (ED-XRF) for the three cores 204, 210, and Kane2B with: (a) boxplot of the distribution of the main elements (wt. %) within the cores, (b)  $\text{Al}_2\text{O}_3$ - $\text{SiO}_2$ - $\text{CaO}$ , and (c)  $\text{Fe}$ - $\text{K}$ - $\text{Ca}$  ternary plots showing the overall composition of the sediment from the three cores: 204, 210, and Kane2B, and average shale composition (Post Archean Australian Shale or PAAS; Pourmand et al., 2012). The black dotted arrows reflect the distribution of the main sources discussed in this study.

and  $\text{Ti}/\text{K}$  ratios to discriminate sediments from sedimentary rocks sources (rich in detrital carbonates, illite, and quartz) and rocks from Precambrian Shield (Inglefield Land; rich in feldspars and quartz).

#### 4.2. Sediment Provenance

The SedUnMixMC program was used to associate long-term changes of the sediment input to changes of sediment sources (based on sources presented in Figure 2). Because these different sediment sources vary geographically and the sediment dynamics did not evolve synchronously throughout the Northwestern Greenland margin during the Holocene, the geochemical and mineralogical results obtained for each sediment core are presented by geographic location. The distribution of mineralogical and geochemical proxies for all cores reveals significant down-core variations (Figures 5–7). Note that the fraction of source not resolved by the SedUnMixMC program is relatively low (ranging from 7 to 27 wt.%).

##### 4.2.1. Core 204: Upernavik Cross-Shelf Trough

In the lowermost part of core 204 (prior  $\sim 7.7$  cal ka BP; Unit 1), the mineralogical and elemental geochemical compositions are dominated by quartz, feldspars, biotite and chlorite, and illites as well as by Si, Al, and K, as denoted by the ratios: quartz/smectite,  $\text{Si}/\text{Ca}$ , and  $\text{K}/\text{Fe}$  (Figure 5). Based on the SedUnMixMC results, this interval is also associated with a high (but decreasing) component of Charnockite (from up to 60 to 30 wt.% of the mineralogical assemblage). After  $\sim 7.7$  cal ka BP (Unit 2a), the sediment input is marked by a progressive increase in pyroxene, kaolinite, and smectite, as well as Ca, Ti, and Fe, as shown by the PCA results and ratio feldspars/pyroxene,  $\text{Si}/\text{Ca}$ , or  $\text{Al}/\text{Ti}$  and associated to a slightly coarser grain size (Figure 5). Likewise, the SedUnMixMC modeling revealed an important increase of the input from the Karat Group (WGMC#1) after 7.7 cal ka BP. A slight and progressive increase of the sediment component from basalts (WGMC#2) is

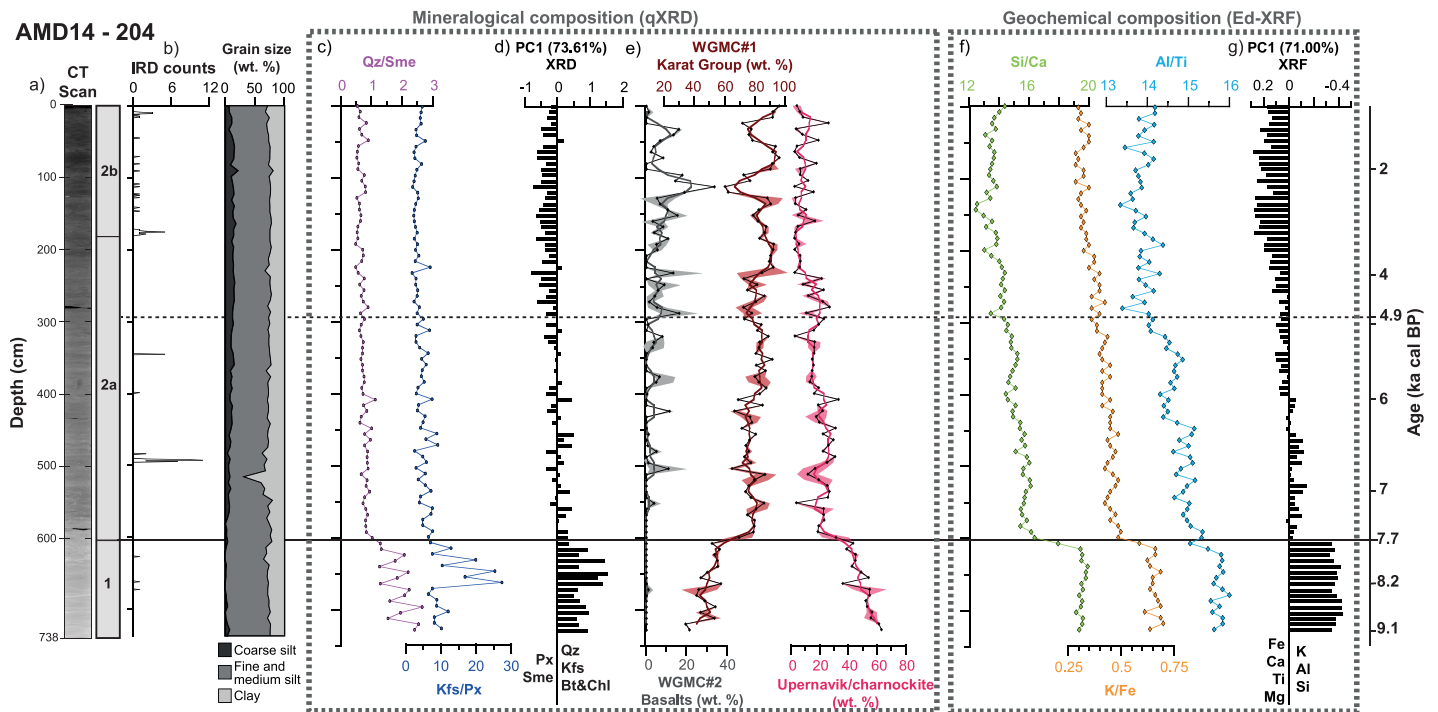


**Figure 5.** Downcore variations of core 204 showing (a) CT scan image and sedimentary units, and (b) ice rafting debris (IRD) counts and grain size distribution (Caron, St-Onge, et al. 2019); (c) ratios quartz/smectite (Qz/Sme) and K-feldspars/pyroxene (Kfs/Px); (d) PC1 scores derived from qXRD log-centered data; (e) SedUnMix results with cumulative proportions of sediment from Charnockite (Upernavik), basalts (WGMC#2), Karrat Group (WGMC#1), and uncertainties for all values are represented by the respective shaded areas (note that 2-theta errors are small compared with samples); (f) from left to right: Si/Ca, K/Fe, and Al/Ti; and (g) PC1 scores derived from ED-XRF log-centered data.

also observed after 7.7 cal ka BP. This input from basalts becomes more important after 4.9 cal ka BP, with the highest concentration (up to 30 wt.%) observed from ~2.3 to 2.0 cal ka BP, and we also note a slightly coarser grain size toward the end of the Holocene (IRDs relatively more abundant in Unit 2b; Figure 5).

#### 4.2.2. Core 210: Melville Bay Cross-Shelf Trough

In core 210 (Figure 6), we observe highest values of quartz (up to 25 wt.%) and plagioclase (up to 35 wt.%) in the glaciomarine sediments prior to ~9.5 cal ka BP (Unit 1), associated with high values of the quartz/clays ratio. Based on the SedUnMixMC results, the sediment input during this interval is variable and alternating from the different sources from Melville Bay surroundings, all originating from the alteration of the Precambrian Shield: Charnockite, WGMC#3, and WGMC#4 (Figure 6). Note that the grain size distribution for this unit does not take into account the coarser materials (sands and gravels), which are visibly present (CT scans and IRD counts; Caron, St-Onge, et al., 2019). From ~9.5 to 8.5 cal ka BP (Unit 2a), we observed the highest concentrations of amphibole and biotite and chlorite (~25–30 wt. % of the mineral assemblage together) and this is reflected by low values of quartz/clays and smectite/amphibole ratios and high values of Ti/Al and Fe/Al ratios. This unit is also associated to a finer grain size and with a dominant source possibly originating from orthogneiss (WGMC#3; ~80 wt. %), although an important part (~20 wt.%) remains unresolved (Figure 6). From ~8.5 to 7.5 cal ka BP (Unit 2b), the SedUnMixMC modeling suggests that sediments are also likely derived from orthogneiss (WGMC#3) and we observe a relatively coarser grain size (Figure 6). However, a marked peak around 192 cm (~7.6 cal ka BP, a thin and coarse rapidly deposited layer) is easily noticeable (Figure 6) and corresponds to a mineral assemblage dominated by quartz, plagioclase, and amphibole (as well as by Si and Ca). This assemblage is represented by high values of quartz/clays ratio and associated to a strong signature of a NW Greenland source (WGMC#4), likely derived from paragneiss or granite (Figure 6). Finally, after 7.5 cal ka BP (Unit 3), we observe an increase of smectite, illite, and amorphous silica (and decrease of Fe), associated to an increase in coarse silts, while the mineral assemblage is again largely associated to a source possibly derived from orthogneiss (WGMC#3, >80 wt.%).

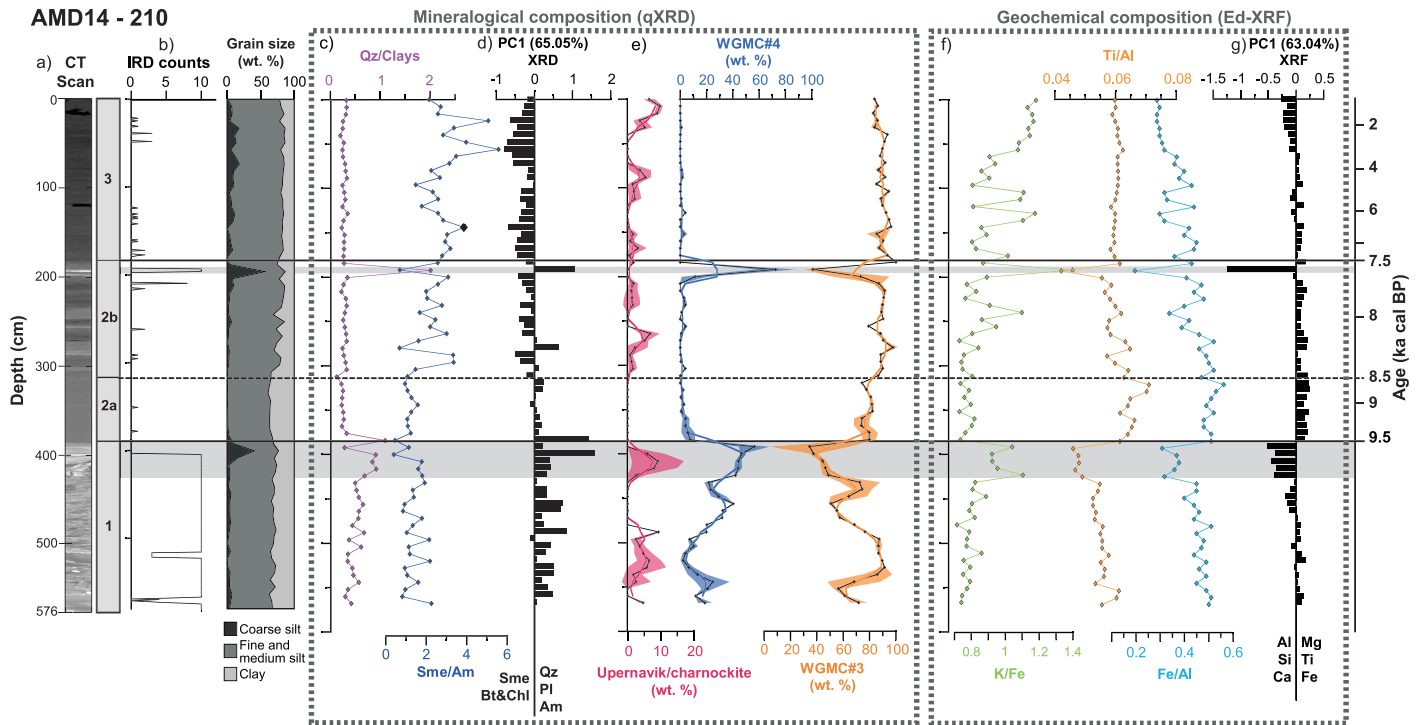


**Figure 6.** Downcore variations of core 210 showing (a) CT scan image and sedimentary units; (b) ice rafting debris (IRD) counts and grain size distribution (Caron, St-Onge, et al. 2019); (c) ratios quartz/total clays (Qz/clays) and smectite/amphibole (Sme/Am); (d) PC1 scores derived from qXRD log-centered data; (e) SedUnMix results with cumulative proportions of sediment from Charnockite (Upervavik), WGMC#3, and WGMC#4 (Precambrian Shield) and uncertainties for all values are represented by the respective shaded areas (note that 2-theta errors are small compared with samples); (f) from left to right: K/Fe, Ti/Al, and Fe/Al; and (g) PC1 scores derived from ED-XRF log-centered data. The gray shadings highlight characteristic changes in the sedimentation.

#### 4.2.3. Core Kane2B: Kane Basin

At the base of core Kane2B (prior 8.95 cal ka BP; first part of Unit 1; Figure 7), we observe increasing concentrations of carbonates associated to an increasing contribution of detrital carbonates (up to 80 wt.% of the mineralogical assemblage). In the second part of Unit 1 (from 8.95 to 8.8 cal ka BP), concentrations of quartz, detrital carbonates, illites, Ca and Mg are high but start decreasing and are associated to a finer grain size (Figure 7). In addition, the SedUnMixMC analysis suggests a still dominant but decreasing source from detrital carbonates, while input from Inglefield Land is increasing (WGMC#3 + 4: 1–40 wt.%) during this interval (Figure 7). From 8.8 to 8.0 cal ka BP (Unit 2), low values of the different ratios reflect an increase of feldspars, amphibole, and biotite and chlorite as well as the Al, Si, K, and Fe. The SedUnMixMC results indicate a stronger sediment input from Inglefield land (WGMC#3 + 4: up to 70 wt% of the mineralogical assemblage) during this period (Figure 7). However, a 20-cm-long clast-rich interval (Unit 2b, 300–320 cm; ~8.3 cal ka BP) rapidly deposited is associated to high concentration of quartz and calcite and Si, Ca, and Ti and demonstrates a different sediment source (detrital carbonate; Figure 7). After 8.0 cal ka BP (Unit 3a), the SedUnMixMC analysis suggests a more important sediment input from detrital carbonates (from 50 to up to 80 wt.% of the mineralogical assemblage). Furthermore, this interval is associated with higher inputs of carbonates, quartz, and illites (higher values of quartz/plagioclase), which correspond to the dominant minerals of the “detrital carbonate” source. Finally, mineral and geochemical assemblages are relatively stable after 5.8 cal ka BP (Unit 3b), with a sediment provenance from 70 to 80 wt.% from detrital carbonates (Ellesmere Island) and ~20/30 wt.% from the Precambrian Shield (Inglefield Land, WGMC#3 + 4) determined by the SedUnMixMC analysis.

## 5. Discussion

The multiproxy approach presented here uses a combination of new mineralogical and geochemical records, associated to grain size and surface water proxies from the same set of samples (Caron, St-Onge, et al., 2019

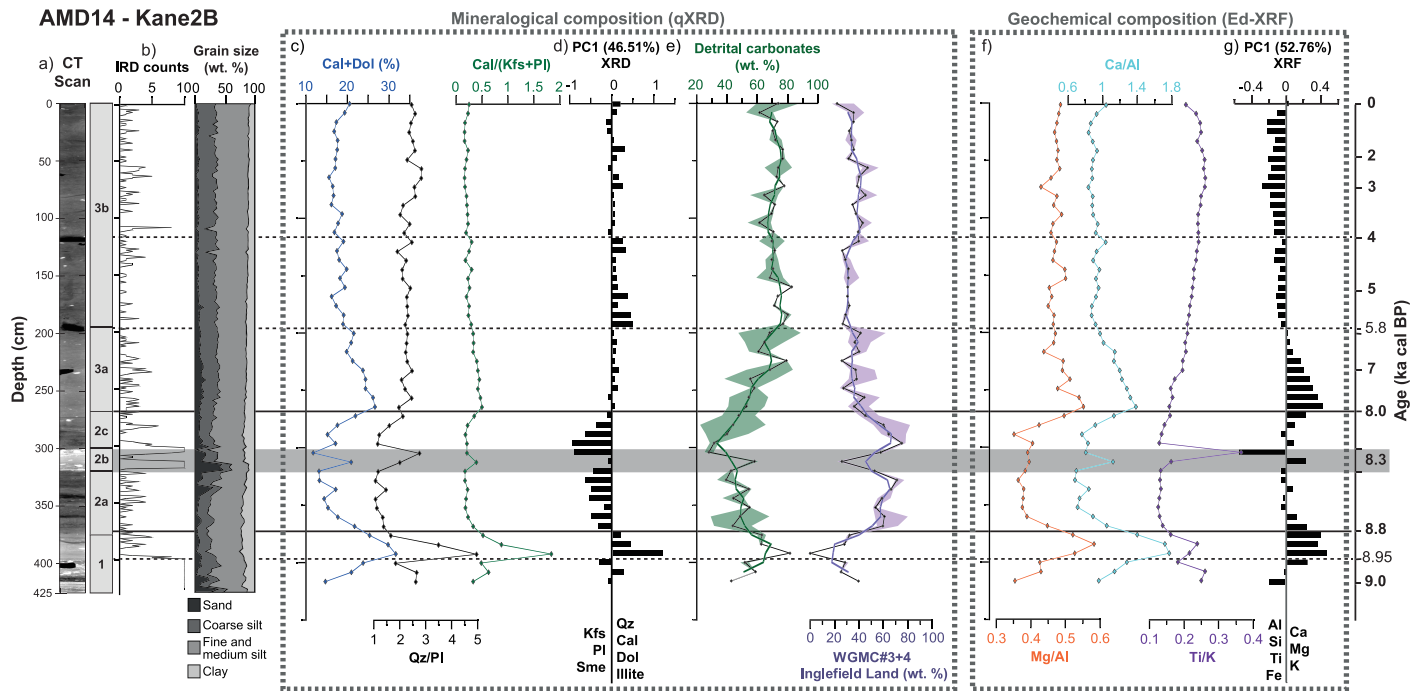


**Figure 7.** Downcore variations of core Kane2B showing (a) CT scan image, sedimentary units; (b) ice rafting debris (IRD) counts and grain size distribution (Caron, St-Onge, et al. 2019); (c) concentration of carbonates (calcite+dolomite, wt.%), ratios quartz/plagioclase (Qz/Pl), and calcite/total feldspars (Cal/Kfs + Pl); (d) PC1 scores derived from qXRD log-centered data; (e) SedUnMix results with cumulative proportions of sediment from the Franklinian basin (detrital carbonates) and Ingfield Land (WGMC#3 + 4) and uncertainties for all values are represented by the respective shaded areas (note that 2-theta errors are small compared with samples); (f) from left to right: ratios Mg/Al, Ca/Al, Ti/K; and (g) PC1 scores derived from ED-XRF log-centered data. The gray shading highlights the rapidly deposited layer.

and Caron, Rochon, et al., 2019) in order to investigate palaeoceanographic changes along the northwestern Greenland margin. Overall, for the three cores, many major elements present good correlations with various minerals identified (Figure S4). For example, Ca is very well correlated with the presence of detrital carbonates in core Kane2B ( $r^2 = 0.93$ ) and K is linked to the presence of K-feldspars and illites in core 204 ( $r^2 = 0.65$ ). Therefore, this connection between mineralogy and major element composition supports and reinforces the use of qXRD to determine the mineralogy of sediment samples (e.g., Eberl & Smith, 2009), as well as the use of SedUnMixMC modeling to estimate the proportions of potential sources for sediments from the northwestern Greenland margin. Variations observed in the mineralogical and geochemical records are discussed below in terms of changes in detrital sediment supply, provenance, and transport and their possible relations with ice stream activities, sea-ice, relative sea level changes, and Holocene climate variability. These results are also compared with  $\delta^{18}\text{O}$  records from the Camp Century ice core and Agassiz ice cap (Vinther et al., 2009). Because the records presented here illustrate different patterns between the cores related to their respective environment, changes are thus discussed in terms of locations for the three cores, in order to provide an intramargin comparison (Upernavik, Melville Bay and Kane Basin).

### 5.1. Upernavik Cross-Shelf Trough (Core 204)

From 9.1 to 7.7 cal ka BP (base of the core), the SedUnMixMC modeling, grain size distribution, high quartz/smectite, Si/Ca, and K/Fe ratios indicate a proximal source of fine-grained sediment originating predominantly from the Upernavik ice stream (40–60 wt.% of Charnockite source; Figures 5 and 8). Previous studies have shown that the Upernavik Glacier had already retreated inland at that time, with age of deglaciation of  $11.3 \pm 0.5$  (outer fjord) and  $9.9 \pm 0.1$  (inner fjord) cal ka BP in the fjord, respectively, for Corbett et al. (2013) and Briner et al. (2013). Moreover, based on a large database of  $^{10}\text{Be}$  ages, Sinclair et al. (2016) demonstrated that most GIS land-based deglaciation occurred after the YD and peaked between 10.5 and 7.0 cal ka BP in West Greenland. This retreat occurred while relative sea level was falling due to

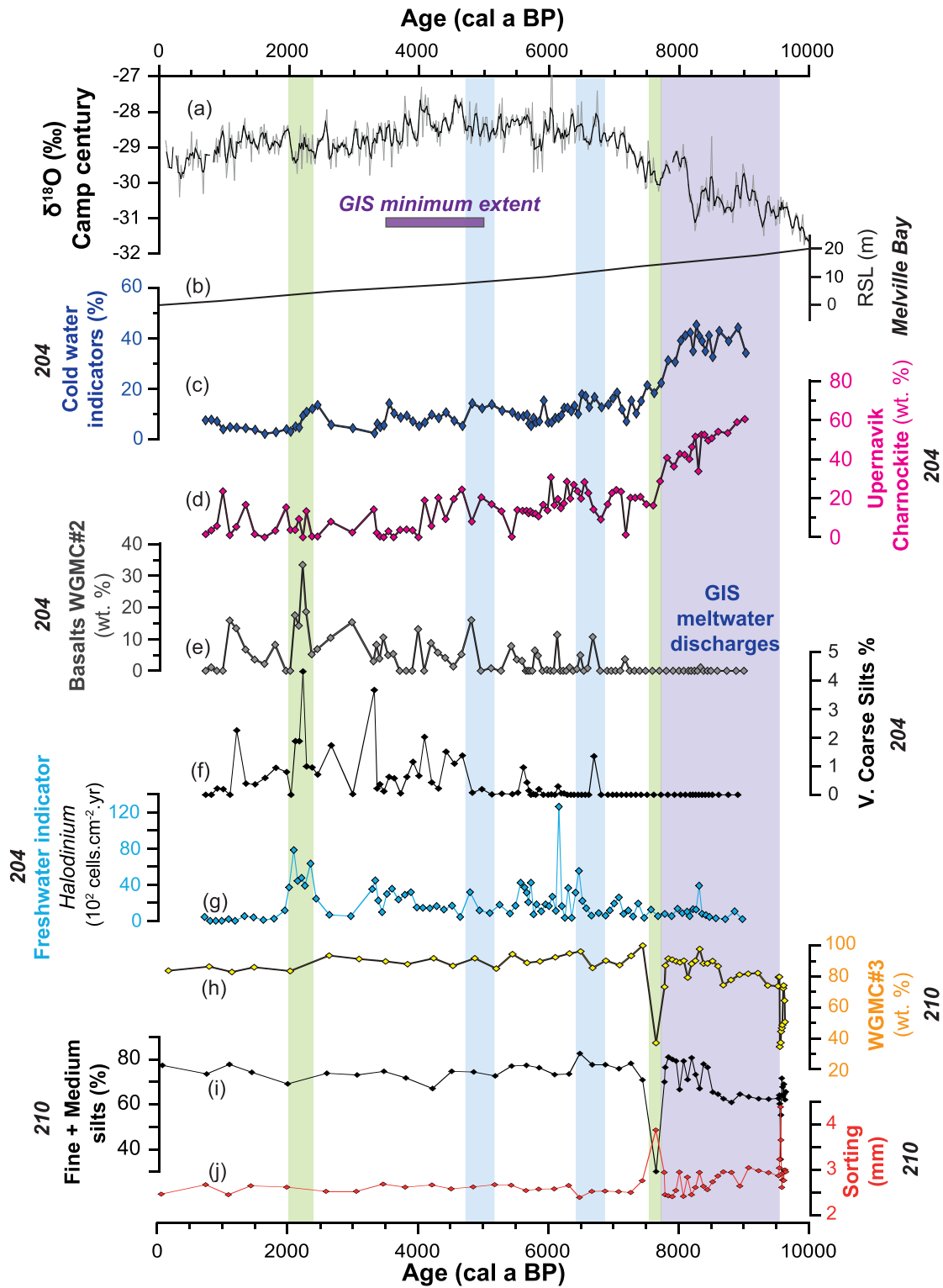


**Figure 8.** Comparison of (a)  $\delta^{18}\text{O}$  from Camp century (Vinther et al., 2009), (b) relative sea level reconstruction for the Melville Bay (approximately, based on Fleming & Lambeck, 2004), (c) dinocyst cold water taxa (%) from Caron, Rochon, et al. (2019), proportions of sediment from (d) Upernavik-Charnokite and (e) basalts (WGMC#2, wt.%) for core 204, (f) amounts of very coarse silts (%) for core 204 (Caron, St-Onge, et al., 2019), (g) freshwater indicator (*Halodinium*) influx from Caron, Rochon, et al. (2019), (h) proportion of sediment from WGMC#3 for core 210, (i) amounts of fine and medium silts (%), and (j) sorting (mm) for core 210. Greenland Ice Sheet (GIS) minimum extent interval from Young and Briner (2015). The light blue shaded areas indicate the cold pulses observed in Caron, Rochon, et al. (2019), and the green shaded areas highlight periods of important change discussed in this study.

glacio-isostatic rebound (Fleming & Lambeck, 2004; Long et al., 2011) and thus could have enhanced sediment remobilization from glacial erosion. Moreover, Jennings et al. (2014) suggested that glacial marine conditions associated to a declining ice sheet mass loss and a high meltwater input remained on the Uummannaq outer shelf until 7.8 cal ka BP. In this context, our detrital proxies support the idea of a fast flowing Upernavik ice stream until  $\sim 7.7$  cal ka BP, associated with a strong meltwater discharge from GIS (e.g., Moros et al., 2016), which brought fine detrital sediment (likely through meltwater plume as the dominant transport process) directly from the fjord to the core site (Figure 10). Comparable results were also reported by Caron, St-Onge, et al. (2019) and Caron, Rochon, et al. (2019) on the same sediment core 204, as reflected by the high abundance of cold-water taxa associated with cold sea-surface conditions, caused by meltwater input (Figure 8c). This hypothesis is also strongly supported by the previous results of Seidenkrantz et al. (2013) suggesting a widespread early Holocene meltwater discharge from GIS, which started prior to 8.6 cal ka BP and ended at  $\sim 7.7$ – $7.5$  cal ka BP.

A major change in sediment provenance was recorded at  $\sim 7.7$  cal ka BP, based on significant variations in the mineralogical and geochemical assemblages (Figures 5 and 8). Indeed, after 7.7 cal ka BP, we observe an important increase of another source with higher concentrations of pyroxene, smectite, and kaolinite (WGMC#1, from  $\sim 50$  to 80 wt.%), as reflected by the different ratios (Figure 5). Andrews et al. (2018) suggested that the detrital source WGMC#1 could be originating from somewhere near Upernavik but could also represent a mixture of sediment sources associated with iceberg rafting, iceberg scouring of the seafloor, and the rainout of suspended sediment. Based on its general composition dominated by feldspars and clays, we hypothesize that the source WGMC#1 was mainly derived from rocks north and south of the Upernavik Charnockite, that is, from the Paleoproterozoic supracrustal rocks (metaturbidites and gneiss) of the Karrat Group formation (Figure 1b; Kalsbeek et al., 1998). Indeed, as the Upernavik ice stream had retreated behind its present margin at that time (Briner et al., 2013), sediments in this region were probably diluted among detrital sediments originating from other West Greenland outlet glaciers (Figure 10).

Furthermore, we observe the progressive increase (from 0 to up to 10 wt.%) of sediments originating from Tertiary basalt outcrops (WGMC#2; Andrews et al., 2018) after 7.7 cal ka BP, as reflected by the K-Feldspar/pyroxene and K/Fe ratios (Figure 5). This increasing contribution of Tertiary basalts (abundant in pyroxene, smectite, and Fe-Ca-Ti), although small, supports an enhanced detrital sediment input via ocean currents, more specifically via the WGC after 7.7 cal ka BP. These findings are consistent with dinoflagellate cyst assemblages (higher abundance of warmer water taxa; Figure 8c) from the same sediment core, which indicate an intensification of WGC strength/influence on the WGS after  $\sim 7.7$  cal ka BP (Caron, Rochon, et al., 2019). This interpretation of a less dominant transport process via ice stream/glacial erosion, favoring a stronger WGC during the middle Holocene period in this area, is also supported by previous studies (e.g., Lloyd et al., 2005; Moros et al., 2016; Perner et al., 2013a, 2013b). Moreover, a reduced meltwater influence during the middle Holocene, as the ice sheet is land-based (Perner et al., 2013b), is also linked to the minimum extent of the northwestern part of GIS, which occurred between  $\sim 5$  and 3.5 cal ka BP (Young & Briner, 2015; Figure 8). However, this minimum extent was possibly preceded by a meltwater pulse or the presence of colder sea-surface conditions (around 5 cal ka BP; Caron, Rochon, et al., 2019; Figure 8). Overall, these results support the idea that sedimentation at the location of core 204 is characterized by a reduced detrital input from meltwater discharges and an enhanced sediment transport by ocean currents (via the WGC) after 7.7 cal ka BP (Figure 10). These changes (perhaps fluctuating) likely resulted in warmer sea surface conditions in this area, favorable for a higher primary productivity during the Mid-Holocene (Caron, Rochon, et al., 2019).

During the late Holocene, glacier growths were observed in West Greenland following the regional Holocene Thermal Maximum (Briner et al., 2016; Schweinsberg et al., 2017, 2019), while in core 204, an increase of very coarse silt concentration (Figure 8f) and of the presence of IRDs (Figure 5) was observed after 4.8 cal ka BP. Interestingly, the highest contribution of basalts (WGMC#2, up to 30 wt.%) in core 204 is found between 2.0 and 2.4 cal ka BP, at the same time as a relatively high sea-ice cover duration ( $\sim 7$  months/year; Caron, Rochon, et al., 2019) and a peak of reworked palynomorphs and freshwater indicator *Halodinium* (Figure 8g). These observations could possibly indicate a stronger input of basalt (via the WGC) due to either a meltwater pulse originating from the Disko/Uummannaq Bays area or drift ice carrying sediments originating from basalts up to the location of core 204. Altogether, this demonstrates a

relationship between the basalt contribution in the sediment composition of core 204 and a coarser grain size and freshwater input, which supports the hypothesis of a stronger input of detrital sediment transported by the ice (drift ice or icebergs) during the Late Holocene (Figure 10).

## 5.2. Melville Bay Cross-Shelf Trough (Core 210)

Core 210 is located in one of the deepest parts (1,155 water depth) of the central Melville Bay cross-shelf trough (e.g., Slabon et al., 2016) and was thus possibly subject to the same processes occurring at the mouths of cross-shelf troughs (e.g., Ó Cofaigh, Andrews, et al., 2013). Moreover, due to its proximity to GIS, we can expect the detrital sediment deposited in this part of the WGS to be primarily derived from the local ice streams (e.g., ice stream pathways in Figure 1b). Andrews et al. (2018) observed that surface sediment in Melville Bay is dominated by two relatively local sources from NW Greenland characterized as WGMC#3 and WGMC#4. The bedrock geology in Melville Bay is largely dominated by reworked Archean gneisses (Figure 1b), and based on respective mineralogical composition, we hypothesized that WGMC#3 is likely derived preferentially from orthogneiss or metagabbro (rich in feldspars, biotite, smectite, and amphibole), while WGMC#4 is rather derived from paragneiss or granite (rich in quartz, feldspars, and amphibole). As highlighted in Figures 6 and 8, changes in the mineralogical composition appears clearly associated with the grain size distribution. Thus, this underline a link between coarser particles and the detrital sediment source WGMC#4, whereas WGMC#3 is rather associated with finer particles.

The base of core 210 (prior to ~9.5 cal ka BP) is characterized by a coarse-grained and poorly sorted deposit corresponding to ice-marginal glaciomarine conditions, and a relatively fast rate of deposition was assumed for this layer (Caron, St-Onge, et al., 2019). This deposit is likely associated to the remobilization of subglacial till or glaciogenic sediments, transported by debris flow (e.g., Ó Cofaigh, Dowdeswell, et al., 2013, 2018). The sediment composition for this unit appears to be fluctuating from a mix of different sources from the West Greenland (mainly WGMC#3 but with significant contribution of WGMC#4), as reflected by the SedUnMixMC results and by quartz/clays, K/Al, and Fe/Al ratios (Figure 6). Small contributions (0–10 wt.%) of sediments originating from the south (Upernavik) are also observed during this interval, suggesting that detrital sediments could also have been transported from the Upernavik ice stream up to the location of core 210 during this period, probably through meltwater discharge. This mixed composition of sediment sources prior to 9.5 cal ka BP is probably due to the important ice streams activity on the WGS, linked to final retreat of the proximal GIS at the end of the deglaciation (e.g., Jennings et al., 2014, 2017; Seidenkrantz et al., 2013). Alternatively, Slabon et al. (2016) suggested the possible presence of an ice dome on the northern intertrough bank of Melville Bay, which could have impacted the sedimentation at the location of core 210 during the early Holocene together with GIS retreat. However, our results cannot support or exclude this hypothesis.

On top of this glaciomarine deposit, a major change occurred in the type and rate of sedimentation, but also in the sediment composition (Figure S1). Indeed, the interval from ~9.5 to 8.5 cal ka BP is marked by higher concentrations of amphibole, biotite and chlorite, and K-Mg-Ti-Fe, noticeable with the quartz/clays, Fe/Al, and Ti/Al ratios (Figure 6). This interval is associated with a significant increase of reworked Archean orthogneiss (WGMC#3) contribution, which remains the largely dominant source afterward (Figures 6 and 8h). Based on the lithology, the finer grain size, and its occurrence right after a glaciomarine deposit (Unit 1), the sedimentary Unit 2a has been attributed to the deposition through suspension settling from turbid meltwater plumes (Caron, St-Onge, et al., 2019). Deglacial ages from the Melville Bay coastline indicate ice sheet margin similar to or behind its present-day position by 9.3–9.0 cal ka BP in the southern part (e.g., Bennike, 2008) and by 9.0–8.5 cal ka BP in the northern part (Kelly, 1980). Thus, we hypothesize that from ~9.5 to 8.5 cal ka, meltwater plumes associated to a strong GIS meltwater discharge could have brought fine-grained detrital sediment mainly from one dominant source derived from gneisses (likely WGMC#3). From ~8.5 to 7.5 cal ka BP, the sedimentation changed to a laminated unit. As suggested in a previous study (Caron, St-Onge, et al., 2019), these laminations could indicate more unstable conditions (successions of rapidly deposited layers from turbidity currents) during this period, but still related to the deposition of sediments suspended in turbid meltwater plumes (e.g., Jenner et al., 2018; Ó Cofaigh et al., 2018; Sheldon et al., 2016). This layer reflects relatively greater distance from the ice margin (compared to Unit 1) but likely still associated to high meltwater discharges from GIS (Moros et al., 2016; Seidenkrantz et al., 2013) and an extended sea-ice cover (e.g., Caron, Rochon, et al., 2019). The fluctuating smectite/amphibole and K/Fe

ratios could reflect different sediment sources for these laminations but could also be simply an effect of grain-size patterns. Indeed, based on the SedUnMixMC results, after ~9.5 cal ka BP, the detrital sediment source throughout the core is dominantly derived from orthogneiss (WGMC#3; Figures 6 and 10). However, we observe one event (peak at ~7.6 cal ka BP) with a clear signature from paragneiss/granite (WGMC#4) similar to the interval prior to 9.5 cal ka BP and a coarser grain size (Figures 6 and 8). This event possibly resulted from an important gravity flow, which brought coarser material up to the location of core 210, from a different sediment source than the rest of Unit 2b (but a source present in Unit 1). Moreover, SedUnMixMC results show small contribution (<10 wt.%) of sediments originating from the south (Upernavik) during this interval (8.5–7.5 cal ka BP), even with the important activity of the Upernavik ice stream recorded in core 204 for this period. Thus, this supports the hypothesis that the major sediment source recorded throughout core 210 (WGMC#3) is a local source from Melville Bay (Figure 10).

During the middle to late Holocene (after 7.5 cal ka BP), the composition of the top unit of core 210 remains relatively homogeneous (as visible on the SedUnMixMC results and quartz/clays and Ti/Al ratios), although K/Fe and smectite/amphibole ratios reveal some variations. Again, one source (WGMC#3, always >80 wt.%) likely directly originating from some of the major ice streams presents around the Melville Bay (e.g., Steenstrup and Kong Oscar glaciers) is largely dominant throughout this interval (Figure 10). However, a slightly higher contribution of detrital sediments from a southern source (Charnockite) is observed toward the end of the Holocene, as reflected by the K/Fe ratio, and could be related to the increasing influence of the WGC while GIS meltwater discharge is reduced (e.g., Lloyd et al., 2005; Moros et al., 2016; Perner et al., 2013a, 2013b).

### 5.3. Kane Basin (Core Kane2B)

As determined by Georgiadis et al. (2018), the base of core Kane2B corresponds to the retreat of grounded ice from the core site (~9.0 cal ka BP). Andrews et al. (1991) established that most of Kane Basin contains a thin cover of silty clay with gravelly IRD that overlies stiff sand and gravelly glacial till, which is present in core Kane2B (Figure 7a). In the lowest part of the core (prior 8.8 cal ka BP), the interplay between sediment inputs from the Franklinian basin (up to 80 wt.%; detrital carbonates) and Inglefield Land (WGMC#3 + 4; gneiss) likely corresponds to major retreat from each side of Kane Basin, either from the IIS (Ellesmere Island, Agassiz Ice cap) or from GIS (Humboldt Glacier; Figures 9 and 10). Thus, based on the SedUnMixMC analysis together with the calcite/total feldspars and Ca/Al ratios (Figure 7), we observe two rapid phases, which occurred after the retreat of grounded ice from the core site. First, an increasing contribution of detrital carbonates until 8.9 cal ka BP was recorded, followed by an increase of sediment input from Inglefield Land (Figure 9). The contribution of sediments from Inglefield Land was dominant (~60–80 wt.%) during the period from ~8.8 to 8.0 cal ka BP, suggesting a more important retreat of the GIS (Humboldt glacier) than IIS (Ellesmere Island). However, this interval was interrupted by an important event at ~8.3 cal ka BP (20-cm-long coarse layer, highlighted in gray in Figure 7) with a mineralogical signature rich in sand (up to 50%; Figure 9g) and detrital carbonates and quartz, as reflected by the quartz/plagioclase and Ca/Al ratios (Figures 7 and 9). As suggested by Georgiadis et al. (2018), this signature could correspond to sediments found in Kennedy Channel (Paleozoic/Franklinian basin detrital carbonates). They interpreted this event as associated to the breaking of the ice saddle in Kennedy Channel, allowing the passage of Arctic water through Nares Strait, which entrained sediment from north of the channel in Kane Basin. This was later discussed by Jennings et al. (2019), proposing the interval from 9.0 to 8.3 cal ka BP for the complete opening of Nares Strait (Figure 9).

After 8.3 cal ka BP, sediment input from detrital carbonates is increasing, while relative sea level is progressively decreasing (due to isostatic adjustment after retreat of ice sheets; Fleming & Lambeck, 2004; Figures 9b and 9c and 10b). This suggests further retreat of the IIS and/or more influence of the Arctic water flow established after the complete opening of Nares Strait (e.g., Georgiadis et al., 2018). Indeed, this enhanced southward flow could have brought more sediments from northernmost Greenland and possibly from the very active Petermann ice stream (e.g., Reilly et al., 2019; Figures 1b and 10b). Furthermore, Jennings et al. (2019) reported relatively high sedimentation rates and deposition of detrital carbonate until 7.2 cal ka BP, while ice margin retreated, in agreement with our results. Besides, Georgiadis et al. (2020) noticed an expanding sea-ice cover in Kane basin between ~7.5 and 5.5 cal ka BP, which remained important afterward. This extended sea-ice cover associated to the enhanced

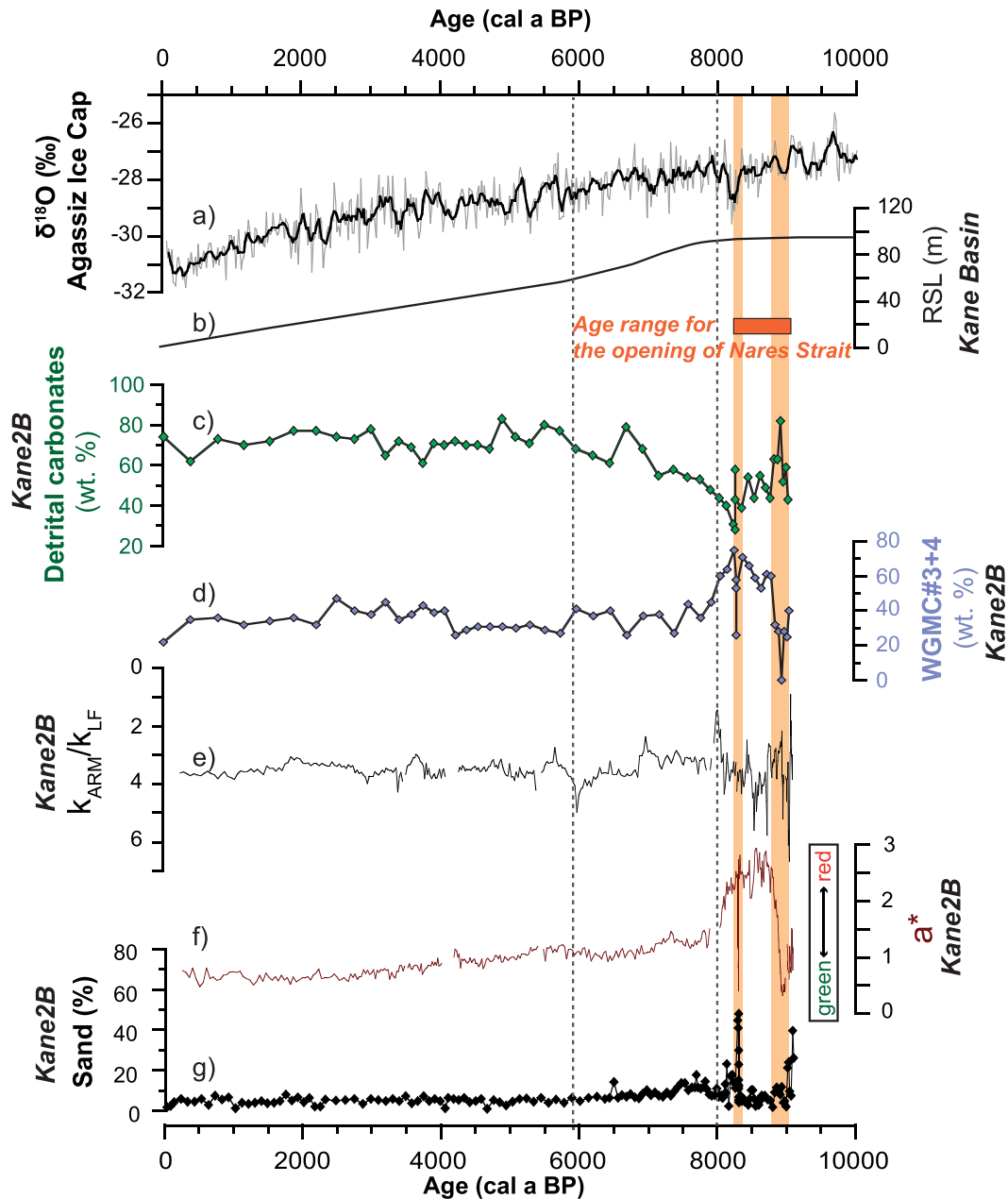


**Figure 9.** Comparison of (a)  $\delta^{18}\text{O}$  from Agassiz Ice cap (Vinther et al., 2009), (b) relative sea level reconstruction for the Kane Basin (approximately, based on Fleming & Lambeck, 2004), (c) proportion of sediment from detrital carbonates, and (d) WGMC#3 + 4 (early Proterozoic gneiss and Inglefield Land) for core Kane2B; (e)  $k_{\text{ARM}}/k_{\text{LF}}$  ratio (magnetic grain size indicator) and (f)  $a^*$  for sediment color (green-red) from Caron, St-Onge, et al. (2019); and (g) sand (%) for core Kane2B from Georgiadis et al. (2018). Interval for the opening of Nares Strait based on Georgiadis et al. (2018) and Jennings et al. (2019) and orange shaded areas highlight rapidly deposited layers likely associated with the opening and discussed in the text. The black dotted lines represent major sedimentological changes in core Kane2B.

southward flow could have triggered an increased detrital sediment input by sea-ice transport, originating from the north. After 5.8 cal ka BP, as revealed by the calcite/total feldspars, Ca/Al, and Ti/K ratios, there is no major changes recorded in the sediment composition, which remains relatively constant until present. This interval is characterized by a mixed provenance from detrital carbonates (~60–70 wt.%, probably from Ellesmere Island but also northernmost Greenland via the BIC) and by Proterozoic gneiss (Inglefield Land, ~30–40 wt.%). The IRD content in core Kane2B (Figure S1) illustrates the continuous calving of icebergs throughout the Holocene (Caron, St-Onge, et al., 2019). Reduced melting of Agassiz ice

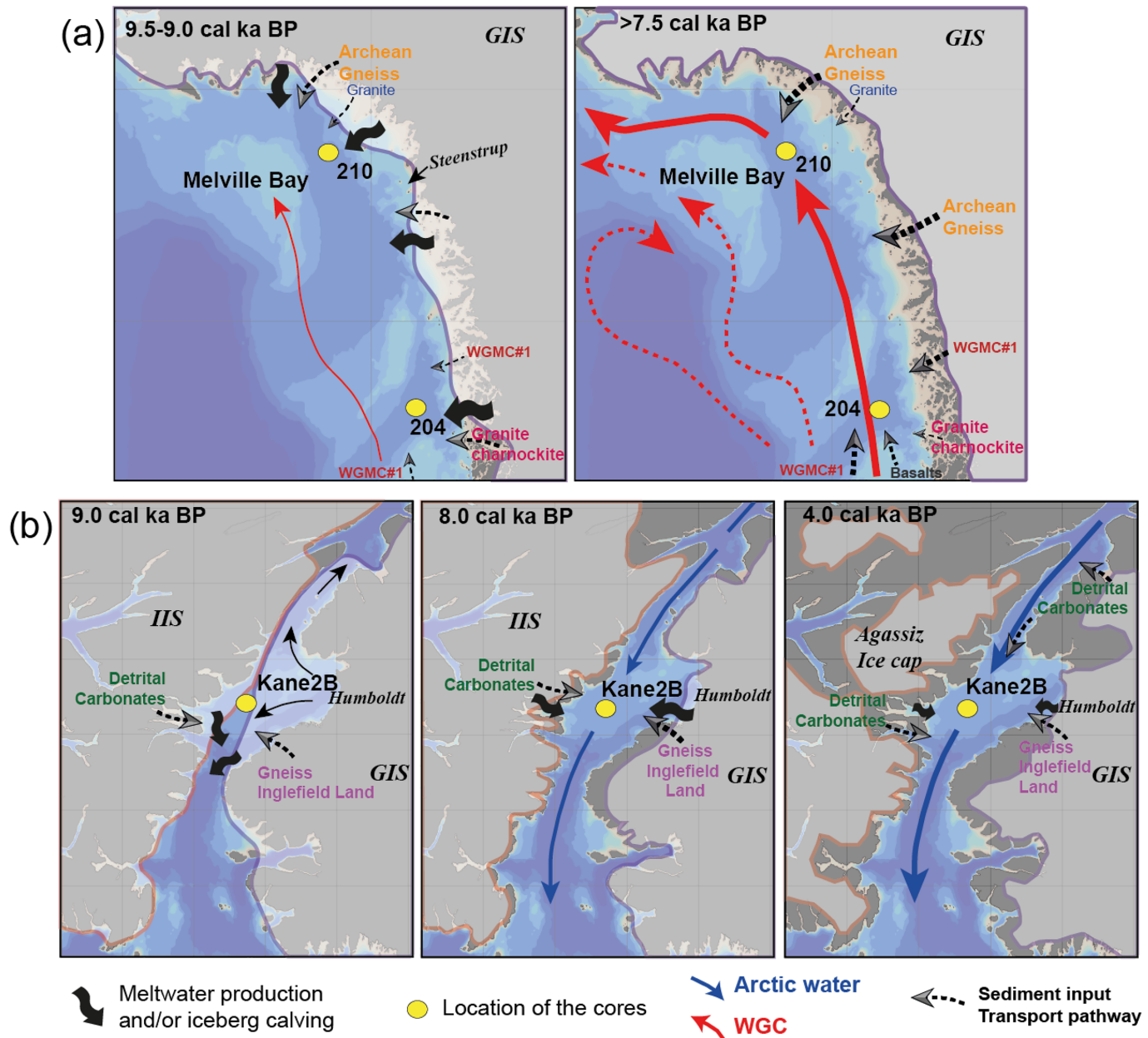


**Figure 10.** Schematic map of (a) the northeastern Baffin Bay around 9.5–9.0 cal ka BP and after 7.5 cal ka BP and (b) Kane Basin around 9.0, 8.0 and 4.0 cal ka BP, representing the evolution of sediment dynamics throughout the Holocene. West Greenland Current (WGC) represented by red arrows and Arctic water southward flow (BIC) represented by blue arrows. Size of arrows represents strength/intensity of the ocean current or sediment source contribution (thin = low, thick = high). Note that sea-ice transport is not represented but plays an important role in these sedimentary transport processes.

Cap was recorded after 4 cal ka BP (Fisher et al., 2012), and Reilly et al. (2019) recorded a stable ice tongue for Petermann glacier after 2 cal ka BP indicating a reduced glacial activity (meltwater discharge and iceberg delivery) during the late Holocene. Furthermore, Jennings et al. (2019) recorded a low sedimentation rate at ~6 cal ka BP and interpreted it as a manifestation of the increasing dominance of the Arctic surface water that developed as isostatic adjustment shallowed channels of the CAA. Overall, our mineralogical and geochemical data suggest that the period after 5.8 cal ka BP likely corresponds to the progressive establishment of the modern sedimentation in this region but reflect minimal changes consistent with the neoglaciation in our marine record. Nevertheless, Late Holocene changes in Kane Basin were observed in the same sediment sequence (core Kane2B) based on micropaleontological proxies (Caron, Rochon, et al., 2019; Georgiadis et al., 2020).

## 6. Conclusions

Results of the mineralogical and geochemical compositions of three sediment cores from the northwestern Greenland margin (cores 204 and 210) and Kane Basin (core Kane2B) revealed different sediment dynamics during the last deglaciation and Holocene. A major change in sediment provenance was recorded in the three regions, occurring around 7.7, 9.5, and 8.0 cal ka BP, respectively, for cores 204, 210, and Kane2B, likely associated with the transition from Early (end of deglaciation) to Mid-Holocene. Moreover, the relative mineralogical and geochemical compositions for the three cores demonstrate a significant downcore variability with evidence of changes in the detrital sediment contributions and transport pathways during the Holocene:

1. In the Upernavik cross-shelf trough (core 204), the base of the core (9.0–7.7 cal ka BP) is dominated by a proximal detrital source (charnockite), suggesting strong calving directly from the Upernavik ice stream at the end of the deglaciation (early Holocene). After 7.7 cal ka BP, results revealed an enhanced contribution from at least two other detrital sediment sources: one originating from regional outlet glaciers from the NW Greenland (WGMC#1) and another source from a southern region (basalts) reflecting an increased influence of ocean currents and sea-ice transport. Hence, with an increased contribution of detrital sediment supply (basalts) from Disko/Uummannaq bays after ~7.7 cal ka BP, these results confirm an intensification in the strength and/or influence of the WGC during the Mid-Holocene.
2. In the central Melville Bay cross-shelf trough (core 210), results revealed a sediment provenance from at least three different sources (granites and gneisses from the Precambrian Shield) prior to ~9.5 cal ka BP, associated to ice-proximal conditions, when the GIS is retreating but still proximal to the core site. After 9.5 cal ka BP, while ice distal conditions are progressively established (once the GIS has retreated close to its actual margin), the sediment provenance is almost exclusively composed of one dominant detrital source (WGMC#3), which likely corresponds to the major outcropping bedrock in this northwestern part of Greenland (Archean orthogneiss).
3. In Kane Basin (core Kane2B), the interplay between sediment inputs from the Franklinian basin (detrital carbonates) and Inglefield Land (gneiss) suggests that sediment dynamics is strongly dependent on the asynchronous retreat of IIS and GIS. Thus, after the retreat of grounded ice from the core site (~9.0 cal ka BP), the detrital sediment supply was firstly affected by the progressive opening of Nares Strait (9.0–8.3 cal ka BP) associated to strong ice streams activity from both IIS and GIS, and establishment of the modern southward flow of Arctic water. Following the opening, detrital sediments originating from Inglefield Land were still relatively abundant until 8.0 cal ka BP. After 8.0 cal ka BP, the sediment provenance is largely dominated by detrital carbonates (Franklinian basin) and remains relatively stable after 5.8 cal ka BP with the establishment of the modern sedimentation.

Overall, this paper provides a better understanding of regional paleoenvironmental changes occurring on the NW Greenland continental margin during the Holocene. The use of a multiproxy approach, achieved by comparing our new mineralogical and geochemical data with existing work on the same cores provided valuable complementary information to better understand the evolution of the sediment dynamics in the NW Greenland margin. Taken as a whole, this paper highlights how oceanographic conditions, ice sheet dynamics, and climatic changes are interconnected between West Greenland, uppermost Baffin Bay, and Nares Strait. Lastly, it demonstrates the importance of mineralogical and geochemical analyses of sediments in differentiating provenance and transport processes changes in glacial marine environments.

## References

- Aitchison, J. (1990). Relative variation diagrams for describing patterns of compositional variability. *Mathematical Geology*, 22(4), 487–511. <https://doi.org/10.1007/BF00890330>
- Aksu, A. E., & Piper, D. J. W. (1987). Late Quaternary sedimentation in Baffin Bay. *Canadian Journal of Earth Sciences*, 24(9), 1833–1846. <https://doi.org/10.1139/e87-174>
- Andrews, J. T. (2019). Baffin Bay/Nares Strait surface (seafloor) sediment mineralogy: Further investigations and methods to elucidate spatial variations in provenance. *Canadian Journal of Earth Sciences*, 56(8), 814–828. <https://doi.org/10.1139/cjes-2018-0207>
- Andrews, J. T., Bjork, A. A., Eberl, D. D., Jennings, A. E., & Verplanck, E. P. (2015). Significant differences in late Quaternary bedrock erosion and transport: East versus West Greenland ~70°N—Evidence from the mineralogy of offshore glacial marine sediments. *Journal of Quaternary Science*, 30(5), 452–463. <https://doi.org/10.1002/jqs.2787>
- Andrews, J. T., & Eberl, D. D. (2011). Surface (sea floor) and near-surface (box cores) sediment mineralogy in Baffin Bay as a key to sediment provenance and ice sheet variations. *Canadian Journal of Earth Sciences*, 48(9), 1307–1328.

## Acknowledgments

We are grateful to the captain, officers, crew, and scientists on board the Canadian Coast Guard Ship Amundsen during the 2014 ArcticNet (Leg 1b) expedition for the recovery of cores 204, 210, and Kane2B. This study was supported by ArcticNet, the Natural Sciences and Engineering Research Council of Canada (NSERC) through Discovery Grants to J.C.M.S., G. S., and A. R., and the CREATE ArcTrain program through a PhD scholarship to the first author. The first author also acknowledges financial support of Québec-Océan. We thank Quentin Beauvais and Marie-Pier St-Onge (ISMER) for technical support in the laboratory. J.C.M.S. thanks Camilla S. Andresen of the Geological Survey of Denmark and Greenland for kindly providing sediment samples from the Upernavik Fjord. All analytical data presented are available electronically in the PANGAEA database (<https://doi.org/10.1594/PANGAEA.908947>). Finally, we thank John T. Andrews (INSTAAR), one anonymous reviewer, and the Associate Editor Guy Harrington for their constructive reviews, which improved the quality of the manuscript, as well as to Ellen Thomas for the editorial work.

- Andrews, J. T., & Eberl, D. D. (2012). Determination of sediment provenance by unmixing the mineralogy of source-area sediments: The "SedUnMix" program. *Marine Geology*, 291, 24–33. <https://doi.org/10.1016/j.margeo.2011.10.007>
- Andrews, J. T., Gibb, O. T., Jennings, A. E., & Simon, Q. (2014). Variations in the provenance of sediment from ice sheets surrounding Baffin Bay during MIS 2 and 3 and export to the Labrador Shelf Sea: Site HU2008029-0008 Davis Strait. *Journal of Quaternary Science*, 29(1), 3–13. <https://doi.org/10.1002/jqs.2643>
- Andrews, J. T., & Jennings, A. E. (2014). Multidecadal to millennial marine climate oscillations across the Denmark Strait (~ 66° N) over the last 2000 cal yr BP. *Climate of the Past*, 10(1).
- Andrews, J. T., Jennings, A. E., MacLean, B., Mudie, P. J., Praeg, D., & Vilks, G. (1991). The surficial geology of the Canadian eastern Arctic and Polar continental shelves. *Continental Shelf Research*, 11(8-10), 791–819.
- Andrews, J. T., Kirby, M. E., Aksu, A., Barber, D. C., & Meese, D. (1998). Late Quaternary detrital carbonate (DC-) layers in Baffin Bay marine sediments (67°–74°N): Correlation with Heinrich events in the North Atlantic? *Quaternary Science Reviews*, 17(12), 1125–1137. [https://doi.org/10.1016/S0277-3791\(97\)00064-4](https://doi.org/10.1016/S0277-3791(97)00064-4)
- Andrews, J. T., Klein, A. J., Jenner, K. A., Jennings, A. E., & Campbell, C. (2018). The variability of Baffin Bay seafloor sediment mineralogy: The identification of discrete glacial sediment sources and application to Late Quaternary downcore analysis. *Canadian Journal of Earth Sciences*, 55(6), 620–639. <https://doi.org/10.1139/cjes-2017-0223>
- Andrews, J. T., Kristjansdottir, G. B., Eberl, D. D., & Jennings, A. (2013). A quantitative X-ray diffraction inventory of the tephra and volcanic glass inputs into the Holocene marine sediment archives off Iceland: A contribution to VAST. *Polar Research*, 32(1), 11,130. <https://doi.org/10.3402/polar.v32i0.11130>
- Andrews, J. T., & Vogt, C. (2014). Source to sink: statistical identification of regional variations in the mineralogy of surface sediments in the western Nordic Seas (58 N–75 N; 10 W–40 W). *Marine Geology*, 357, 151–162. <https://doi.org/10.1016/j.quascirev.2013.05.025>
- Batchelor, C. L., & Dowdeswell, J. A. (2014). The physiography of High Arctic cross-shelf troughs. *Quaternary Science Reviews*, 92, 68–96. <https://doi.org/10.1016/j.quascirev.2013.05.025>
- Batchelor, C. L., Dowdeswell, J. A., & Rignot, E. (2018). Submarine landforms reveal varying rates and styles of deglaciation in North-West Greenland fjords. *Marine Geology*, 402, 60–80. <https://doi.org/10.1016/j.margeo.2017.08.003>
- Bennike, O. (2008). An early Holocene Greenland whale from Melville Bugt, Greenland. *Quaternary Research*, 69(1), 72–76. <https://doi.org/10.1016/j.yqres.2007.10.004>
- Briner, J. P., Håkansson, L., & Bennike, O. (2013). The deglaciation and neoglaciation of Upernavik Isstrøm, Greenland. *Quaternary Research*, 80(3), 459–467. <https://doi.org/10.1016/j.yqres.2013.09.008>
- Briner, J. P., McKay, N. P., Axford, Y., Bennike, O., Bradley, R. S., de Vernal, A., et al. (2016). Holocene climate change in Arctic Canada and Greenland. *Quaternary Science Reviews*, 147, 340–364.
- Caron, M., Montero-Serrano, J.-C., St-Onge, G., Rochon, A. (2019). Bulk mineralogy and elemental geochemistry from sediment cores AMD14-204, AMD14-210 and AMD14-Kane2B (northwestern Greenland margin). *PANGAEA*, <https://doi.org/10.1594/PANGAEA.908947>
- Caron, M., Rochon, A., Montero-Serrano, J.-C., & St-Onge, G. (2019). Evolution of sea-surface conditions on the northwestern Greenland margin during the Holocene. *Journal of Quaternary Science*, 34(7), 569–580. <https://doi.org/10.1002/jqs.3146>
- Caron, M., St-Onge, G., Montero-Serrano, J. C., Rochon, A., Georgiadis, E., Giraudeau, J., & Massé, G. (2019). Holocene chronostratigraphy of northeastern Baffin Bay based on radiocarbon and palaeomagnetic data. *Boreas*, 48(1), 147–165. <https://doi.org/10.1111/bor.12346>
- Comas, M., & Thió-Henestrosa, S. (2011). CoDaPack 2.0: A stand-alone multi-platform compositional software. In J. J. Egozcue, R. Tolosana-Delgado, & M. I. Ortego (Eds.), *CoDaWork'11: 4th International Workshop on Compositional Data Analysis*. Girona, Spain: Saint Feliu de Guixols.
- Corbett, L. B., Bierman, P. R., Graly, J. A., Neumann, T. A., & Rood, D. H. (2013). Constraining landscape history and glacial erosivity using paired cosmogenic nuclides in Upernavik, northwest Greenland. *Bulletin*, 125(9–10), 1539–1553.
- Cordua, A. M. (2016). Development of the late Holocene deglacial environment in Upernavik Isfjord, Northwest Greenland. Msc thesis, Univ. of Copenhagen.
- Dawes, P. R. (1997). The proterozoic thule supergroup, Greenland and Canada: History, lithostratigraphy and development. *Geology of Greenland Survey Bulletin*, 174, 150.
- Dawes, P. R. (2009). Precambrian - Palaeozoic geology of Smith Sound, Canada and Greenland: Key constraint to palaeogeographic reconstructions of northern Laurentia and the North Atlantic region. *Terra Nova*, 21(1), 1–13. <https://doi.org/10.1111/j.1365-3121.2008.00845.x>
- Dawes, P. R., Frisch, T., Garde, A. A., Iannelli, T. R., Ineson, J. R., Jensen, S. M., et al. (2000). Kane Basin 1999: Mapping, stratigraphic studies and economic assessment of Precambrian and Lower Palaeozoic provinces in north-western Greenland. *Geology of Greenland Survey Bulletin*, 186, 11–28.
- Deschamps, C. E., Montero-Serrano, J. C., & St-Onge, G. (2018). Sediment provenance changes in the western Arctic Ocean in response to ice rafting, sea level, and oceanic circulation variations since the last deglaciation. *Geochemistry, Geophysics, Geosystems*, 19(7), 2147–2165. <https://doi.org/10.1029/2017GC007411>
- Dowdeswell, J. A., Hogan, K. A., Ó Cofaigh, C., Fugelli, E. M. G., Evans, J., & Noormets, R. (2014). Late Quaternary ice flow in a West Greenland fjord and cross-shelf trough system: Submarine landforms from Rink Isbrae to Uummannaq shelf and slope. *Quaternary Science Reviews*, 92, 292–309. <https://doi.org/10.1016/j.quascirev.2013.09.007>
- Dyke, A. S., Andrews, J. T., Clark, P. U., England, J. H., Miller, G. H., Shaw, J., & Veillette, J. J. (2002). The Laurentide and Innuitian ice sheets during the Last Glacial Maximum. *Quaternary Science Reviews*, 21(1-3), 9–31. [https://doi.org/10.1016/S0277-3791\(01\)00095-6](https://doi.org/10.1016/S0277-3791(01)00095-6)
- Eberl, D. D. (2003). User guide to RockJock—A program for determining quantitative mineralogy from X-ray diffraction data. *USGS Open File Report, OF, 03-78*, 40. <https://doi.org/10.3133/ofr200378>
- Eberl, D. D., & Smith, D. B. (2009). Mineralogy of soils from two continental-scale transects across the United States and Canada and its relation to soil geochemistry and climate. *Applied Geochemistry*, 24(8), 1394–1404. <https://doi.org/10.1016/j.apgeochem.2009.04.010>
- England, J. H., Atkinson, N., Bednarski, J., Dyke, A. S., Hodgson, D., & Ó Cofaigh, C. (2006). The Innuitian Ice Sheet: Configuration, dynamics and chronology. *Quaternary Science Reviews*, 25(7-8), 689–703. <https://doi.org/10.1016/j.quascirev.2005.08.007>
- Escher, J. C., & Pulvertaft, T. C. R. (1995). *Geological map of Greenland, 1:2 500 000*. Geological Survey of Greenland: Copenhagen.
- Fisher, D., Zheng, J., Burgess, D., Zdanowicz, C., Kinnard, C., Sharp, M., & Bourgeois, J. (2012). Recent melt rates of Canadian arctic ice caps are the highest in four millennia. *Global and Planetary Change*, 84, 3–7.
- Fleming, K., & Lambeck, K. (2004). Constraints on the Greenland Ice Sheet since the Last Glacial Maximum from sea-level observations and glacial-rebound models. *Quaternary Science Reviews*, 23(9-10), 1053–1077.

- Funder, S., Kjeldsen, K. K., Kjær, K. H., & Ó Cofaigh, C. (2011). The Greenland Ice Sheet during the past 300,000 years: A review, in Quaternary Glaciations, Extent and Chronology. In J. Ehlers, P. L. Gibbard, P. D. Hughes (Eds.), Part IV, *A Closer Look, Developments in Quaternary Sciences* (Vol. 15, pp. 699–713). Amsterdam: Elsevier. <https://doi.org/10.1016/B978-0-444-53447-7.00050-7>
- Gamboa, A., Montero-Serrano, J. C., St-Onge, G., Rochon, A., & Desiage, P. A. (2017). Mineralogical, geochemical, and magnetic signatures of surface sediments from the Canadian Beaufort Shelf and Amundsen Gulf (Canadian Arctic). *Geochemistry, Geophysics, Geosystems*, 18(2), 488–512. <https://doi.org/10.1002/2016GC006477>
- Georgiadis, E., Giraudeau, J., Jennings, A., Limoges, A., Jackson, R., Ribeiro, S., & Massé, G. (2020). Local and regional controls on Holocene sea ice dynamics and oceanography in Nares Strait. *Northwest Greenland. Marine Geology*, 422, 106115. <https://doi.org/10.1016/j.margeo.2020.106115>
- Georgiadis, E., Giraudeau, J., Martínez, P., Lajeunesse, P., St-Onge, G., Schmidt, S., & Massé, G. (2018). Deglacial to postglacial history of Nares Strait, Northwest Greenland: A marine perspective. *Climate of the Past Discussions*, 14(12), 1991–2010. <https://doi.org/10.5194/cp-2018-78>
- Hammer, Ø., Harper, D. A. T., & Ryan, P. D. (2001). PAST: Paleontological statistics software package for education and data analysis. *Palaeontologia Electronica*, 4(1), 9.
- Henderson, G., & Pulvertaft, T. C. R. (1967). The stratigraphy and structure of the Precambrian rocks of the Umanak area, West Greenland. Fr. Bagges Kgl. Hofbogtrykkeri.
- Hiscott, R. N., Aksu, A. E., & Nielsen, O. B. (1989). Provenance and dispersal patterns, Pliocene-Pleistocene section at site 645, Baffin Bay. In *Proc. Ocean Drill. Program Sci. Results* (Vol. 105, pp. 31–52).
- Howat, I. M., Joughin, I., Fahnestock, M. A., Smith, B. E., & Scambos, T. A. (2008). Synchronous retreat and acceleration of southeast Greenland outlet glaciers 2000–06: Ice dynamics and coupling to climate. *Journal of Glaciology*, 54(187), 646–660. <https://doi.org/10.3189/002214308786570908>
- Jackson, R., Carlson, A. E., Hillaire-Marcel, C., Wacker, L., Vogt, C., & Kucera, M. (2017). Asynchronous instability of the North American-Arctic and Greenland Ice Sheets during the last deglaciation. *Quaternary Science Reviews*, 164, 140–153. <https://doi.org/10.1016/j.quascirev.2017.03.020>
- Jakobsson, M., Long, A., Ingólfsson, Ó., Kjær, K. H., & Spielhagen, R. F. (2010). New insights on Arctic Quaternary climate variability from palaeo-records and numerical modelling. *Quaternary Science Reviews*, 29(25–26), 3349–3358. <https://doi.org/10.1016/j.quascirev.2010.08.016>
- Jakobsson, M., Mayer, L., Coakley, B., Dowdeswell, J. A., Forbes, S., Fridman, B., et al. (2012). The international bathymetric chart of the Arctic Ocean (IBCAO) version 3.0. *Geophysical Research Letters*, 39(12), n/a. <https://doi.org/10.1029/2012GL052219>
- Jenner, K. A., Campbell, D. C., & Piper, D. J. W. (2018). Along-slope variations in sediment lithofacies and depositional processes since the Last Glacial Maximum on the northeast Baffin margin, Canada. *Marine Geology*, 405, 92–107. <https://doi.org/10.1016/j.margeo.2018.07.012>
- Jennings, A. E., Andrews, J. T., Oliver, B., Walczak, M., & Mix, A. (2019). Retreat of the Smith Sound ice stream in the Early Holocene. *Boreas*, 48(4), 825–840.
- Jennings, A. E., Andrews, J. T., Ó Cofaigh, C., St-Onge, G., Sheldon, C., Belt, S. T., et al. (2017). Ocean forcing of ice sheet retreat in central West Greenland from LGM through deglaciation. *Earth and Planetary Science Letters*, 472, 1–13. <https://doi.org/10.1016/j.epsl.2017.05.007>
- Jennings, A. E., Andrews, J. T., Ó Cofaigh, C., St-Onge, G., Belt, S., Cabedo-Sanz, P., et al. (2018). Baffin Bay paleoenvironments in the LGM and HSI: Resolving the ice-shelf question. *Marine Geology*, 402, 5–16. <https://doi.org/10.1016/j.margeo.2017.09.002>
- Jennings, A., Sheldon, C., Cronin, T. M., Francus, P., Stoner, J., & Andrews, J. T. (2011). The Holocene history of Nares Strait: Transition from Glacial Bay to Arctic-Atlantic Throughflow. *Oceanography*, 24(3), 26–41. <https://doi.org/10.5670/oceanog.2011.52>
- Jennings, A. E., Walton, M. E., Ó Cofaigh, C., Kilfeather, A., Andrews, J. T., Ortiz, J. D., et al. (2014). Paleoenvironments during Younger Dryas-E arly Holocene retreat of the Greenland Ice Sheet from outer Disko Trough, central west Greenland. *Journal of Quaternary Science*, 29(1), 27–40. <https://doi.org/10.1002/jqs.2652>
- Joughin, I., Das, S. B., King, M. A., Smith, B. E., Howat, I. M., & Moon, T. (2008). Seasonal speedup along flank of the Greenland Ice Sheet the Western. *Science*, 320(5877), 781–783. <https://doi.org/10.1126/science.1153288>
- Joughin, I., Smith, B. E., Howat, I. M., Moon, T., & Scambos, T. A. (2016). A SAR record of early 21st century change in Greenland. *Journal of Glaciology*, 62(231), 62–71. <https://doi.org/10.1017/jog.2016.10>
- Kalsbeek, F., Pulvertaft, T. C. R., & Nutman, A. P. (1998). Geochemistry, age and origin of metagreywackes from the Palaeoproterozoic Karrat Group, Rinkian belt, West Greenland. *Precambrian Research*, 91(3–4), 383–399. [https://doi.org/10.1016/S0301-9268\(98\)00059-X](https://doi.org/10.1016/S0301-9268(98)00059-X)
- Kelly, M. (1980). Preliminary investigations of the Quaternary of Melville Bugt and Dundas, north-west Greenland. *Rapport Gronlands Geologiske Undersogelse*, 100, 33–38.
- Larsen, L. M., & Pedersen, A. K. (2009). Petrology of the Paleocene picrites and flood basalts on Disko and Nuussuaq, West Greenland. *Journal of Petrology*, 50(9), 1667–1711. <https://doi.org/10.1093/petrology/egp048>
- Lloyd, J., Moros, M., Perner, K., Telford, R. J., Kuijpers, A., Jansen, E., & McCarthy, D. (2011). A 100 yr record of ocean temperature control on the stability of Jakobshavn Isbrae, West Greenland. *Geology*, 39(9), 867–870. <https://doi.org/10.1130/G32076.1>
- Lloyd, J. M., Park, L. A., Kuijpers, A., & Moros, M. (2005). Early Holocene palaeoceanography and deglacial chronology of Disko Bugt, west Greenland. *Quaternary Science Reviews*, 24(14–15), 1741–1755. <https://doi.org/10.1016/j.quascirev.2004.07.024>
- Long, A. J., Woodroffe, S. A., Roberts, D. H., & Dawson, S. (2011). Isolation basins, sea-level changes and the Holocene history of the Greenland Ice Sheet. *Quaternary Science Reviews*, 30(27–28), 3748–3768.
- MacLean, B., Williams, G. L., Srivastava, S. P., & Keen, M. J. (1990). Geology of Baffin Bay and Davis Strait. *Geology of Canada*, 2, 293–348.
- Marlowe, J. I. (1966). Mineralogy as an indicator of long-term current fluctuations in Baffin Bay. *Canadian Journal of Earth Sciences*, 3(2), 191–201. <https://doi.org/10.1139/e66-015>
- Miller, G. H., Wolfe, A. P., Briner, J. P., Sauer, P. E., & Nesje, A. (2005). Holocene glaciation and climate evolution of Baffin Island, Arctic Canada. *Quaternary Science Reviews*, 24(14–15), 1703–1721. <https://doi.org/10.1016/j.quascirev.2004.06.021>
- Montero-Serrano, J. C., Palarea-Albaladejo, J., Martín-Fernández, J. A., Martínez-Santana, M., & Gutiérrez-Martín, J. V. (2010). Sedimentary chemofacies characterization by means of multivariate analysis. *Sedimentary Geology*, 228(3–4), 218–228. <https://doi.org/10.1016/j.sedgeo.2010.04.013>
- Moros, M., Lloyd, J. M., Perner, K., Krawczyk, D., Blanz, T., de Vernal, A., et al. (2016). Surface and sub-surface multi-proxy reconstruction of middle to late Holocene palaeoceanographic changes in Disko Bugt, West Greenland. *Quaternary Science Reviews*, 132, 146–160. <https://doi.org/10.1016/j.quascirev.2015.11.017>

- Müller, J., & Stein, R. (2014). High-resolution record of late glacial and deglacial sea ice changes in Fram Strait corroborates ice-ocean interactions during abrupt climate shifts. *Earth and Planetary Science Letters*, *403*, 446–455.
- Noël, B., van de Berg, W. J., Lhermitte, S., Wouters, B., Schaffer, N., & van den Broeke, M. R. (2018). Six decades of glacial mass loss in the Canadian Arctic Archipelago. *Journal of Geophysical Research: Earth Surface*, *123*(6), 1430–1449.
- Oakey, G. N., & Chalmers, J. A. (2012). A new model for the Paleogene motion of Greenland relative to North America: plate reconstructions of the Davis Strait and Nares Strait regions between Canada and Greenland. *Journal of Geophysical Research: Solid Earth*, *117*(B10).
- Ó Cofaigh, C., Hogan, K. A., Jennings, A. E., Callard, S. L., Dowdeswell, J. A., Noormets, R., & Evans, J. (2018). The role of meltwater in high-latitude trough-mouth fan development: The Disko Trough-Mouth Fan, West Greenland. *Marine Geology*, *402*, 17–32. <https://doi.org/10.1016/j.margeo.2018.02.001>
- Ó Cofaigh, C., Taylor, J., Dowdeswell, J. A., & Pudsey, C. J. (2003). Palaeo-ice streams, trough mouth fans and high-latitude continental slope sedimentation. *Boreas*, *32*(1), 37–55. <https://doi.org/10.1080/03009480310001858>
- Ó Cofaigh, C., Andrews, J. T., Jennings, A. E., Dowdeswell, J. A., Hogan, K. A., Kilfeather, A. A., & Sheldon, C. (2013). Glacimarine lithofacies, provenance and depositional processes on a West Greenland trough-mouth fan. *Journal of Quaternary Science*, *28*(1), 13–26. <https://doi.org/10.1002/jqs.2569>
- Ó Cofaigh, C., Dowdeswell, J. A., Jennings, A. E., Hogan, K. A., Kilfeather, A., Hiemstra, J. F., et al. (2013). An extensive and dynamic ice sheet on the West Greenland shelf during the last glacial cycle. *Geology*, *41*(2), 219–222. <https://doi.org/10.1130/G33759.1>
- Parnell, J., Bowden, S., Andrews, J. T., & Taylor, C. (2007). Biomarker determination as a provenance tool for detrital carbonate events (Heinrich events?): Fingerprinting Quaternary glacial sources into Baffin Bay. *Earth and Planetary Science Letters*, *257*(1–2), 71–82.
- Pedersen, G. K., & Pulvertaft, T. C. R. (1992). The nonmarine Cretaceous of the West Greenland Basin, onshore West Greenland. *Cretaceous Research*, *13*(3), 263–272.
- Pendleton, S., Miller, G., Lifton, N., & Young, N. (2019). Cryosphere response resolves conflicting evidence for the timing of peak Holocene warmth on Baffin Island, Arctic Canada. *Quaternary Science Reviews*, *216*, 107–115. <https://doi.org/10.1016/j.quascirev.2019.05.015>
- Perner, K., Moros, M., Jennings, A., Lloyd, J. M., & Knudsen, K. L. (2013a). Holocene palaeoceanographic evolution off West Greenland. *The Holocene*, *23*(3), 374–387. <https://doi.org/10.1177/0959683612460785>
- Perner, K., Moros, M., Snowball, I. A. N., Lloyd, J. M., Kuijpers, A., & Richter, T. (2013b). Establishment of modern circulation pattern at c. 6000 cal a BP in Disko Bugt, central West Greenland: Opening of the Vaigat Strait. *Journal of Quaternary Science*, *28*(5), 480–489. <https://doi.org/10.1002/jqs.2638>
- Pourmand, A., Dauphas, N., & Ireland, T. J. (2012). A novel extraction chromatography and MC-ICP-MS technique for rapid analysis of REE, Scand Y: Revising Cf-chondrite and post-Archean Australian Shale (PAAS) abundances. *Chemical Geology*, *291*, 38–54. <https://doi.org/10.1016/j.chemgeo.2011.08.011>
- Reilly, B. T., Stoner, J. S., Mix, A. C., Walczak, M. H., Jennings, A., Jakobsson, M., et al. (2019). Holocene break-up and reestablishment of the Petermann Ice Tongue, Northwest Greenland. *Quaternary Science Reviews*, *218*, 322–342. <https://doi.org/10.1016/j.quascirev.2019.06.023>
- Rignot, E., Fenty, I., Xu, Y., Cai, C., Velicogna, I., Ó Cofaigh, C., et al. (2016). Bathymetry data reveal glaciers vulnerable to ice-ocean interaction in Uummannaq and Vaigat glacial fjords, west Greenland. *Geophysical Research Letters*, *43*(6), 2667–2674. <https://doi.org/10.1002/2016GL067832>
- Rignot, E., Koppes, M., & Velicogna, I. (2010). Rapid submarine melting of the calving faces of West Greenland glaciers. *Nature Geoscience*, *3*(3), 187–191. <https://doi.org/10.1038/ngeo765>
- Schweinsberg, A. D., Briner, J. P., Licciardi, J. M., Bennike, O., Lifton, N. A., Graham, B. L., et al. (2019). Multiple independent records of local glacier variability on Nuussuaq, West Greenland, during the Holocene. *Quaternary Science Reviews*, *215*, 253–271. <https://doi.org/10.1016/j.quascirev.2019.05.007>
- Schweinsberg, A. D., Briner, J. P., Miller, G. H., Bennike, O., & Thomas, E. K. (2017). Local glaciation in West Greenland linked to North Atlantic Ocean circulation during the Holocene. *Geology*, *45*(3), 195–198. <https://doi.org/10.1130/G38114.1>
- Seidenkrantz, M. S., Ebbesen, H., Aagaard-Sorensen, S., Moros, M., Lloyd, J. M., Olsen, J., et al. (2013). Early Holocene large-scale meltwater discharge from Greenland documented by foraminifera and sediment parameters. *Palaeogeography, Palaeoclimatology, Palaeoecology*, *391*(Part A), 71–81. <https://doi.org/10.1016/j.palaeo.2012.04.006>
- Serreze, M. C., & Stroeve, J. (2015). Arctic sea ice trends, variability and implications for seasonal ice forecasting. *Philosophical Transactions of the Royal Society A*, *373*(2045), 20140159. <https://doi.org/10.1098/rsta.2014.0159>
- Sheldon, C., Jennings, A. E., Andrews, J. T., Ó Cofaigh, C., Hogan, K. A., Dowdeswell, J. A., & Seidenkrantz, M.-S. (2016). Ice stream retreat following the LGM and onset of the west Greenland current in Uummannaq Trough, west Greenland. *Quaternary Science Reviews*, *147*, 27–46. <https://doi.org/10.1016/j.quascirev.2016.01.019>
- Simon, Q. (2013). Propriétés magnétiques, minéralogiques et sédimentologiques des sédiments profonds de la baie de Baffin: chronologie et dynamique des glaciers ouest groenlandais, innuitiens et laurentidiens au cours de la dernière glaciation.
- Simon, Q., Hillaire-Marcel, C., St-Onge, G., & Andrews, J. T. (2014). North-eastern Laurentide, western Greenland and southern Innuitian ice stream dynamics during the last glacial cycle. *Journal of Quaternary Science*, *29*(1), 14–26. <https://doi.org/10.1002/jqs.2648>
- Simon, Q., Thouveny, N., Bourlès, D. L., Nuttin, L., Hillaire-Marcel, C., & St-Onge, G. (2016). Authigenic <sup>10</sup>Be/<sup>9</sup>Be ratios and <sup>10</sup>Be-fluxes (230Thxs-normalized) in central Baffin Bay sediments during the last glacial cycle: Palaeoenvironmental implications. *Quaternary Science Reviews*, *140*, 142–162. <https://doi.org/10.1016/j.quascirev.2016.03.027>
- Sinclair, G., Carlson, A. E., Mix, A. C., Lecavalier, B. S., Milne, G., Mathias, A., et al. (2016). Diachronous retreat of the Greenland Ice Sheet during the last deglaciation. *Quaternary Science Reviews*, *145*, 243–258. <https://doi.org/10.1016/j.quascirev.2016.05.040>
- Slabon, P., Dorschel, B., Jokat, W., Myklebust, R., Hebbeln, D., & Gebhardt, C. (2016). Greenland Ice Sheet retreat history in the northeast Baffin Bay based on high-resolution bathymetry. *Quaternary Science Reviews*, *154*, 182–198. <https://doi.org/10.1016/j.quascirev.2016.10.022>
- Straneo, F., & Heimbach, P. (2013). North Atlantic warming and the retreat of Greenland's outlet glaciers. *Nature*, *504*(7478), 36–43.
- Tang, C. C. L., Ross, C. K., Yao, T., Petrie, B., DeTracey, B. M., & Dunlap, E. (2004). The circulation, water masses and sea-ice of Baffin Bay. *Progress in Oceanography*, *63*(4), 183–228. <https://doi.org/10.1016/j.pocean.2004.09.005>
- Thomas, E. K., Briner, J. P., Ryan-Henry, J. J., & Huang, Y. (2016). A major increase in winter snowfall during the middle Holocene on western Greenland caused by reduced sea ice in Baffin Bay and the Labrador Sea. *Geophysical Research Letters*, *43*(10), 5302–5308. <https://doi.org/10.1002/2016GL068513>
- Thrane, K., Baker, J., Connelly, J., & Nutman, A. (2005). Age, petrogenesis and metamorphism of the syn-collisional Proven Igneous Complex, West Greenland. *Contributions to Mineralogy and Petrology*, *149*(5), 541–555.

- von Eynatten, H., Barceló-Vidal, C., & Pawlowsky-Glahn, V. (2003). Modelling compositional change: The example of chemical weathering of granitoid rocks. *Mathematical Geology*, 35(3), 231–251. <https://doi.org/10.1023/A:1023835513705>
- von Eynatten, H., Tolosana-Delgado, R., Karius, V., Bachmann, K., & Caracciolo, L. (2016). Sediment generation in humid Mediterranean setting: Grain-size and source-rock control on sediment geochemistry and mineralogy (Sila Massif, Calabria). *Sedimentary Geology*, 336, 68–80. <https://doi.org/10.1016/j.sedgeo.2015.10.008>
- Winsor, K., Carlson, A. E., Caffee, M. W., & Rood, D. H. (2015). Rapid last-deglacial thinning and retreat of the marine-terminating southwestern Greenland ice sheet. *Earth and Planetary Science Letters*, 426, 1–12.
- Young, N. E., & Briner, J. P. (2015). Holocene evolution of the western Greenland ice sheet: Assessing geophysical ice-sheet models with geological reconstructions of ice-margin change. *Quaternary Science Reviews*, 114, 1–17. <https://doi.org/10.1016/j.quascirev.2015.01.018>